PHYSICAL REVIEW D **76,** 094012 (2007)

High p_T top quarks at the CERN Large Hadron Collider

U. Baur*
Department of Physics, State University of New York, Buffalo, New York 14260, USA

L. H. Orr†
Department of Physics and Astronomy, University of Rochester, Rochester, New York 14627, USA
(Received 13 July 2007; published 9 November 2007)

Many new physics models predict resonances with masses in the TeV range which decay into a pair of top quarks. With its large cross section, $t\bar{t}$ production at the Large Hadron Collider (LHC) offers an excellent opportunity to search for such particles. The identification of very energetic top quarks is crucial in such an analysis. We consider in detail the $t\bar{t} \to \ell^{\pm}\nu b\bar{b}q\bar{q}'$ ($\ell = e, \mu$) final state for high p_T top quarks. In this phase space region, two or more of the final state quarks can merge into a single jet due to the large Lorentz boost of the parent top quark. As a result, a large fraction of $t\bar{t} \to \ell^{\pm}\nu b\bar{b}q\bar{q}'$ events with an invariant mass in the TeV region contains less than four observable jets. Requiring one or two tagged b-quarks, we calculate the W + jets, Wb + jets, $Wb\bar{b}$ + jets, Wbt, and single top plus jets backgrounds for these final states, and identify cuts which help to suppress them. In particular, we discuss whether a cut on the jet invariant mass may be useful in reducing the background in the $\ell\nu$ + 2 jets channel. We also investigate how next-to-leading-order QCD corrections affect high p_T top quark production at the LHC. We find that the $\ell\nu$ + 2 jets and $\ell\nu$ + 3 jets final states with one or two b-tags will significantly improve the chances for discovering new heavy particles in the $t\bar{t}$ channel at the LHC.

DOI: 10.1103/PhysRevD.76.094012 PACS numbers: 14.65.Ha, 13.85.Qk

I. INTRODUCTION

The Large Hadron Collider (LHC) is scheduled to have its first physics run in 2008. Investigating jet, weak boson, and top quark production are some of the goals of the 2008 run. Top pair production at the LHC, with a cross section which is about a factor 100 larger than at the Fermilab Tevatron, will make it possible to precisely determine the top quark properties [1]. It also offers an excellent chance to search for new physics in the early operational phase of the LHC. Once the LHC reaches design luminosity, $t\bar{t}$ production will provide access to new phenomena in the multi-TeV region. Many extensions of the standard model (SM) predict particles which decay into $t\bar{t}$ pairs, and thus show up as resonances in the $t\bar{t}$ invariant mass, $m(t\bar{t})$, distribution. The masses of these particles are typically in the TeV range. For example, topcolor [2,3] and little Higgs [4–6] models predict weakly coupled new vector bosons, models with extra dimensions [7–9] can have Kaluza-Klein (KK) excitations of the graviton [10,11] the weak [9,12] and the strong gauge bosons [13–20] which couple to top quarks, while massive axial vector bosons appear in torsion gravity models [21]. Resonances in the $t\bar{t}$ channel also occur in technicolor [22,23], chiral color [24], and models with a strong $SU(3) \times SU(3)$ gauge symmetry [25,26]. In some models [10,13–16], the couplings of the new particles to light quarks and gluons are suppressed, and the $t\bar{t}$ final state becomes their main discovery channel.

Top quarks decay either hadronically, $t \to Wb \to bq\bar{q}'$ ($q, q' = u, d, s, c$), or semileptonically, $t \to Wb \to b\ell\nu$ ($\ell = e, \mu$; decays with τ leptons in the final state are ignored here). Pair production of top quarks thus results in so-called "dilepton + jets" events, $t\bar{t} \to \ell^{\pm}\nu_{\ell}\ell'^{\mp}\nu_{\ell'}b\bar{b}$, "lepton + jets" events, $t\bar{t} \to \ell^{\pm}\nu b\bar{b}q\bar{q}'$, or the "all-hadronic," $t\bar{t} \to b\bar{b}$ + 4 quarks, final state. For sufficiently small top quark transverse momenta, $p_T(t)$, a substantial fraction of $t\bar{t}$ events has a number of isolated jets within the p_T and rapidity range covered by the detector which is equal to or greater (when large angle, hard QCD radiation is included) than the number of quarks in the final state. This is reflected in the standard $t\bar{t}$ selection criteria of the LHC experiments. For example, to identify lepton + jets events, ATLAS and CMS require an isolated charged lepton, missing transverse momentum, and at least four isolated hadronic jets. For events with more than four jets, the four leading (highest transverse momentum) jets are selected. Of these four jets two have to be tagged as b-quarks [27,28]. The main background in this case originates from $Wb\bar{b}$ + 2 jets and W + 4 jets production, and is quite small [27,28].

While the standard top quark selection criteria work well for top quark transverse momenta less than a few hundred GeV and $t\bar{t}$ invariant masses below 1 TeV, they are not adequate in the TeV region where signatures from new $t\bar{t}$ resonances are expected. In this region the top quark decay products are highly boosted and thus almost collinear. This frequently results in nonisolated leptons and/or merged or overlapping jets for lepton + jets and all-hadronic $t\bar{t}$ events, i.e. the number of jets may be smaller than the number of final state quarks. Furthermore, the b-tagging efficiency in the TeV region may be significantly smaller than at low energies [6,14,19]. Imposing standard $t\bar{t}$ selection criteria for very energetic top quarks therefore may

*baur@ubhex.physics.buffalo.edu
†orr@pas.rochester.edu

dramatically reduce the observable cross section for $t\bar{t}$ invariant masses in the TeV range, and severely limit the sensitivity of the LHC experiments to $t\bar{t}$ resonances in this range.

Extending the selection criteria to include topologies with fewer jets is an obvious strategy for improving the selection efficiency for very energetic top quarks. On the other hand, this may significantly increase the background. For example, for lepton + jets events where all three quarks originating from the hadronically decaying top quark merge into one jet, $Wb\bar{b}$ and Wjj production contributes to the background. These processes occur at a lower order in perturbation theory than $pp \to Wb\bar{b} +$ 2 jets and $pp \to W + 4$ jets and therefore are potentially more dangerous. Relaxing the selection criteria further by requiring only one tagged b-quark in $t\bar{t}$ events may partially compensate for the reduced b-tagging efficiency at very high energies. However, this will also increase the reducible background where a light quark or gluon jet is misidentified as a b-quark. Since the mistagging probability worsens significantly with energy [6,19], the background for final states with only one b-tag is potentially much larger than if two b-tags are required.

The importance of modifying the selection criteria for very energetic top quarks to optimize the search for KK excitations of the gluon in bulk Randall-Sundrum models has been discussed in Refs. [13,14]. In this paper we follow a more general approach and investigate whether it is feasible to improve the $t\bar{t}$ selection efficiency for very energetic top quarks. In Sec. II we discuss the signatures and the selection of $t\bar{t}$ events with high p_T top quarks in the lepton + jets, dilepton + jets, and the all-hadronic decay modes. We also investigate how next-to-leading-order (NLO) QCD corrections affect the cross section for the lepton + jets channel in the phase space region of interest. The main result of Sec. II is that the $\ell\nu + 2$ jets and $\ell\nu +$ 3 jets final state topologies with one or two tagged b-jets offer the best chances to improve the $t\bar{t}$ selection efficiency. In Sec. III we calculate the differential cross sections of the SM background processes as a function of the $t\bar{t}$ invariant mass and the top quark transverse momentum for these final states. More precisely, we consider the $Wb\bar{b}$ + jets, $(Wb + W\bar{b})$ + jets, W + jets, $(t + \bar{t})$ + jets, $(t\bar{b} + \bar{t}b) +$ jets, Wbt, and $Wt(j)$ backgrounds. We also show that cluster transverse mass and invariant mass cuts are sufficient to control the background at large values of $m(t\bar{t})$ and $p_T(t)$. Of particular interest for suppressing the background is a cut on the jet invariant mass in Wjj and $(t + \bar{t})j$ production. In Sec. IV we investigate the efficiency of such a cut. Our conclusions are presented in Sec. V.

Considering the $\ell\nu + 2$ jets and $\ell\nu + 3$ jets final state topologies with one or two tagged b-jets in $t\bar{t}$ production is, of course, not new. These final states have been successfully used to search for the top quark in run 1 of the Fermilab Tevatron [29,30] where it was essential to maximize the number of signal events. This is also the case at the LHC in the high invariant mass and p_T region when searching for signals of new physics. However, there is an important difference between the top quark search at the Tevatron and the search for new physics in the $t\bar{t}$ channel at the LHC. At the Tevatron, most $\ell\nu + 2$ jets and $\ell\nu +$ 3 jets $t\bar{t}$ events are the result of one or two jets which do not pass the p_T and rapidity cuts imposed. For very energetic top quarks at the LHC, jet merging is the main source of such events.

All tree level (NLO QCD) cross sections in this paper are computed using CTEQ6L1 (CTEQ6M) [31] parton distribution functions (PDFs). For the CTEQ6L1 PDFs, the strong coupling constant is evaluated at leading order with $\alpha_s(M_Z^2) = 0.130$. The factorization and renormalization scales for the calculation of the $t\bar{t}$ signal are set equal to $\sqrt{m_t^2 + p_T^2(t)}$, where $m_t = 173$ GeV is the top quark mass. The value of the top quark mass chosen is consistent with the most recent experimental data [32]. The choice of factorization and renormalization scales of the background processes is discussed in Sec. III. The standard model (SM) parameters used in all tree-level calculations are [33]

$$G_\mu = 1.166\,39 \times 10^{-5}\ \text{GeV}^{-2}, \tag{1}$$

$$M_Z = 91.188\ \text{GeV}, \qquad M_W = 80.419\ \text{GeV}, \tag{2}$$

$$\sin^2\theta_W = 1 - \left(\frac{M_W^2}{M_Z^2}\right), \qquad \alpha_{G_\mu} = \frac{\sqrt{2}}{\pi} G_F \sin^2\theta_W M_W^2, \tag{3}$$

where G_F is the Fermi constant, M_W and M_Z are the W and Z boson masses, θ_W is the weak mixing angle, and α_{G_μ} is the electromagnetic coupling constant in the G_μ scheme.

II. DETECTING VERY ENERGETIC TOP QUARKS

A. The lepton + jets final state at leading order

We begin our discussion by examining the lepton + jets final state in more detail. The dilepton + jets and the all-hadronic final states will be discussed in Sec. II D. Approximately 30% of all top quark pairs yield lepton + jets events. We calculate the SM $t\bar{t} \to \ell\nu b\bar{b}q\bar{q}'$ cross section at leading order (LO), including all decay correlations. Top quark and W decays are treated in the narrow width approximation. We require that both b-quarks are tagged with a constant efficiency of $\epsilon_b = 0.6$ [27,28] and that there are two additional jets in the event which are not tagged. We sum over electron and muon final states and impose the following acceptance cuts on $\ell\nu b\bar{b}jj$ events at the LHC (pp collisions at $\sqrt{s} = 14$ TeV):

$$p_T(\ell) > 20\ \text{GeV}, \qquad |\eta(\ell)| < 2.5, \tag{4}$$

$$p_T(j) > 30\ \text{GeV}, \qquad |\eta(j)| < 2.5, \tag{5}$$

$$p_T(b) > 30 \text{ GeV}, \qquad |y(b)| < 2.5, \tag{6}$$

$$\not{p}_T > 40 \text{ GeV}. \tag{7}$$

Here, η (y) is the pseudorapidity (rapidity), $\ell = e$, μ, and $\not{p}_T$ is the missing transverse momentum originating from the neutrino in $t \to b\ell\nu$ which escapes undetected. We include minimal detector effects via Gaussian smearing of parton momenta according to ATLAS [27] expectations, and take into account the b-jet energy loss via a parametrized function. Details are given in the Appendix. Charged leptons are assumed to be detected with an efficiency of $\epsilon_\ell = 0.85$. All numerical results presented in this paper include the appropriate combination of b-tagging and lepton detection efficiencies unless specified otherwise. In addition to the cuts listed in Eqs. (4)–(7), the LHC experiments will also impose isolation cuts on all final state objects except the missing transverse momentum by requiring the separation in pseudorapidity—azimuth space to be larger than a minimum value, $R_{\min}$:

$$\Delta R = [(\Delta\eta)^2 + (\Delta\Phi)^2]^{1/2} > R_{\min}. \tag{8}$$

The minimum separation usually is in the range $R_{\min} = 0.4$–0.7.

The cuts listed in Eqs. (4)–(7) are sufficient for the LHC operating at low luminosity, $\mathcal{L} \leq 10^{33}$ cm^{-2} s^{-1}. They should be tightened somewhat for luminosities closer to the design luminosity, $\mathcal{L} = 10^{34}$ cm^{-2} s^{-1}. However, this will have only a small effect on the cross section in the TeV region on which we concentrate in this paper.

New particles which decay into a pair of top quarks lead to resonances in the $t\bar{t}$ invariant mass distribution and to a Jacobian peak in the top quark transverse momentum distribution. In the following we therefore concentrate on these observables. Since the neutrino escapes undetected, $m(t\bar{t})$ cannot be directly reconstructed. However, assuming that the charged lepton and the missing transverse momentum come from a W boson with a fixed invariant mass $m(\ell\nu) = M_W$, it is possible to reconstruct the longitudinal momentum of the neutrino, $p_L(\nu)$, albeit with a twofold ambiguity. In our calculations of the $m(t\bar{t})$ distribution in the lepton + jets final state, we reconstruct the $t\bar{t}$ invariant mass using both solutions for $p_L(\nu)$ with equal weight. The energy loss of the b-quarks slightly distorts the $\not{p}_T$ distribution. As a result, the quadratic equation for $p_L(\nu)$ does not always have a solution. Events for which this is the case are discarded in our analysis. This results in a $\approx 10\%$ reduction of the $t\bar{t}$ cross section in the $m(t\bar{t})$ distribution. More advanced algorithms [34] improve the reconstruction of the mass of the new physics signal, however, they have little effect on the shape of the SM $m(t\bar{t})$ distribution.

In order to reconstruct the t or $\bar{t}$ transverse momentum, one has to correctly assign the b and $\bar{b}$ momenta to the parent top or antitop quark. Since it is impossible to determine the b-charge on an event-by-event basis, we combine $\not{p}_T$, $p_T(\ell)$, and the transverse momentum of the tagged b-jet with the smaller separation from the charged lepton to form the transverse momentum of the semileptonically decaying top quark. The p_T's of the two nontagged jets and the other b-jet form the transverse momentum of the hadronically decaying top.[1] We find that the reconstructed and true top quark transverse momentum distributions are virtually identical except for transverse momenta below 50 GeV where deviations at the few percent level are observed.

The angle between the momentum vector of a top quark decay particle and the flight direction of the parent t quark tends to be small for very energetic top quarks, due to the large Lorentz boost. Imposing a standard isolation cut on the charged lepton and the jets in $t\bar{t} \to \ell\nu b\bar{b}jj$ events thus significantly reduces the $t\bar{t}$ cross section at large values of $m(t\bar{t})$ and $p_T(t)$. This is seen in Fig. 1, where we show the $t\bar{t}$ invariant mass and the $p_T(t \to b\ell\nu)$ distribution for the $\ell\nu b\bar{b}jj$ final state and three choices of $R_{\min}$, with $R_{\min} = 0$ corresponding to no isolation cut being imposed. The smallest differential cross section shown in Fig. 1, 10^{-7} pb/GeV, corresponds to one event in a 100 GeV bin for an integrated luminosity of 100 fb^{-1}. It can be viewed as a crude measure of the LHC reach once it operates at design luminosity. At LO, the transverse momentum distributions of the t and the $\bar{t}$ quark are identical. We therefore do not show the transverse momentum distribution of the hadronically decaying top quark in Fig. 1. The figure demonstrates that the isolation cut greatly reduces the cross section in the TeV region, in particular, in the $p_T(t)$ distribution.

Events which fail the isolation cut either have a charged lepton which is embedded inside a jet, or some of the final state quark jets merge and one observes lepton + jets events with fewer than four jets. Events with nonisolated leptons are difficult to utilize. In most $t\bar{t}$ lepton + jets events with a nonisolated lepton, the lepton is embedded in the b-jet which originates from the same parent top quark. Such a lepton can easily be confused with a charged lepton originating from semileptonic b-decay. Furthermore, such events look similar to QCD $b\bar{b}$ + jets events where one or more badly mismeasured jets result in a significant amount of missing transverse momentum. Finally, since the neutrino is not required to be isolated, the ΔR cut affects the $t \to b\ell\nu$ decay much less than $t \to bjj$. Trying to utilize lepton + jets events with fewer than four jets thus is potentially more beneficial than attempting to use events where the lepton is not isolated.

In the following we therefore focus on $\ell\nu + n$ jets events with $n < 4$. If we require two b-tagged jets, the $n = 1$ final state does not contribute. This leaves the $\ell\nu + 2$ jets and $\ell\nu + 3$ jets final states.

[1] Alternatively, one could select the bjj combination which minimizes $|m(bjj) - m_t|$ [35].

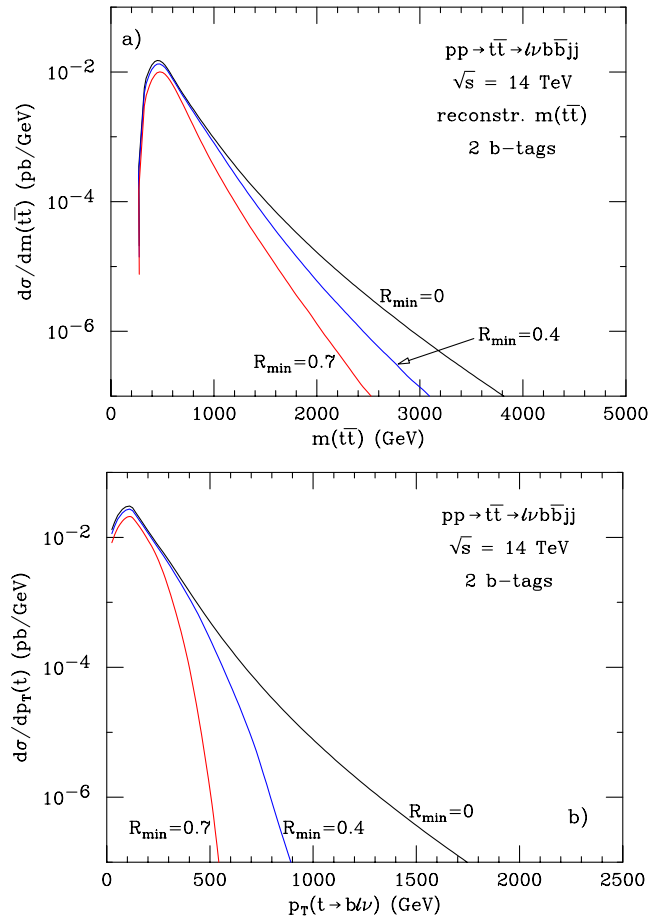

FIG. 1 (color online). The LO $pp \to t\bar{t} \to \ell\nu b\bar{b}jj$ differential cross section at the LHC for three choices of $R_{\rm min}$ as a function of (a) the reconstructed $t\bar{t}$ invariant mass, and (b) the reconstructed p_T of the semileptonically decaying top quark. The cuts imposed are listed in Eqs. (4)–(7).

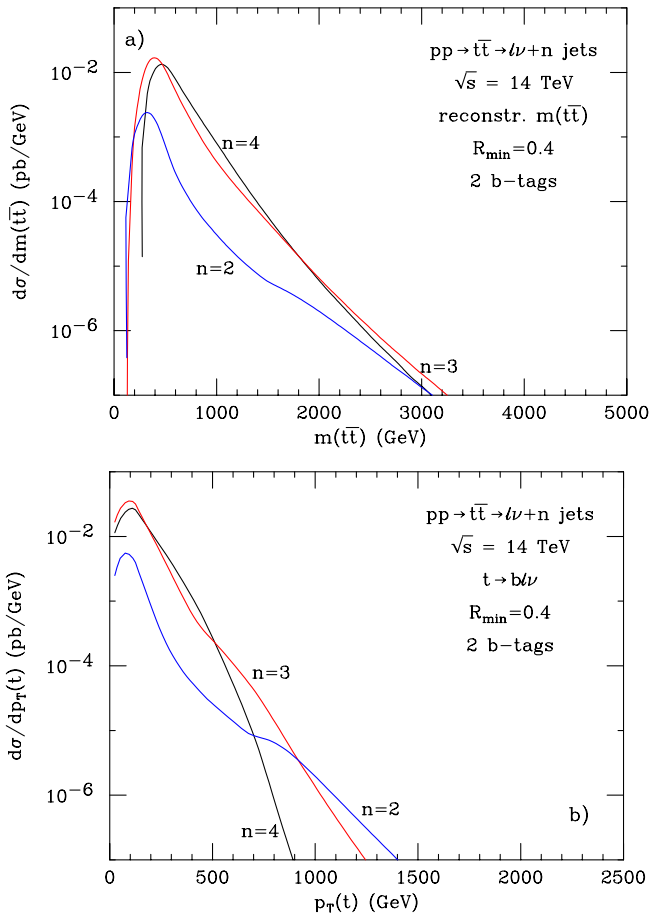

FIG. 2 (color online). The LO $pp \to t\bar{t} \to \ell\nu + n$ jets differential cross section at the LHC as a function of (a) the reconstructed $t\bar{t}$ invariant mass, and (b) the reconstructed p_T of the semileptonically decaying top quark. Shown are the cross sections for two (blue), three (red), and four (black) jets in the final state. Two of the jets are assumed to be b-tagged. The cuts imposed are listed in Eqs. (4)–(7). In addition an isolation cut [see Eq. (8)] with $R_{\rm min} = 0.4$ is imposed and jets with $\Delta R < 0.4$ are merged.

We calculate LO $pp \to t\bar{t} \to \ell\nu + n$ jets production by merging light quark jets from $W \to q\bar{q}'$ and b-quark jets if

$$\Delta R(i, j) < 0.4, \tag{9}$$

$i, j = q, q', b$. If a b-quark jet and a light quark jet merge, their momenta are combined into a b-jet. Jets are counted and used in the reconstruction of $m(t\bar{t})$ if they satisfy Eqs. (5) and (6) after merging. The $m(t\bar{t})$ and $p_T(t \to b\ell\nu)$ differential cross sections for $pp \to t\bar{t} \to \ell\nu + n$ jets with two b-tags and $n = 2, 3$ are shown in Figs. 2(a) and 2(b) respectively. For comparison, we also show the $\ell\nu + 4$ jets distributions. Taking into account the $\ell\nu +$ 2 jets and $\ell\nu + 3$ jets final states is seen to increase the cross section for very large values of $m(t\bar{t})$ by more than a factor of 3. The effect is even more pronounced in the $p_T(t)$ distribution where the 2 jet and 3 jet final states extend the range which is accessible from 900 GeV to about 1.4 TeV. The LO results shown in Fig. 2 are, of course, expected to be somewhat modified by QCD corrections. The QCD corrections for the lepton + jets final state topologies will be discussed in more detail in Sec. II B. They do not qualitatively change the results presented in Fig. 2.

At small transverse momenta and invariant masses, most of the 2 jet and 3 jet final states originate from 4 jet events where one or both light quark jets do not pass the p_T and rapidity cuts of Eq. (5). With increasing energies, more and more $\ell\nu + n$ jet events with $n = 2, 3$ contain jets which originate from jet merging. This is most pronounced in the $n = 2$ case where it leads to a shoulder in the differential cross section at $m(t\bar{t}) \approx 1.5$ TeV and $p_T(t) \approx 700$ GeV. At large invariant masses or p_T's, $t\bar{t} \to \ell\nu + 2$ jet events originate almost exclusively from the merging of all three quarks in $t \to bq\bar{q}'$ into one "t-jet" which, however, is tagged as a b-jet. The invariant mass of such jets, which is close to m_t, and their shower profile [36] are potential tools for discriminating signal and QCD $Wjj/Wb\bar{b}$ background

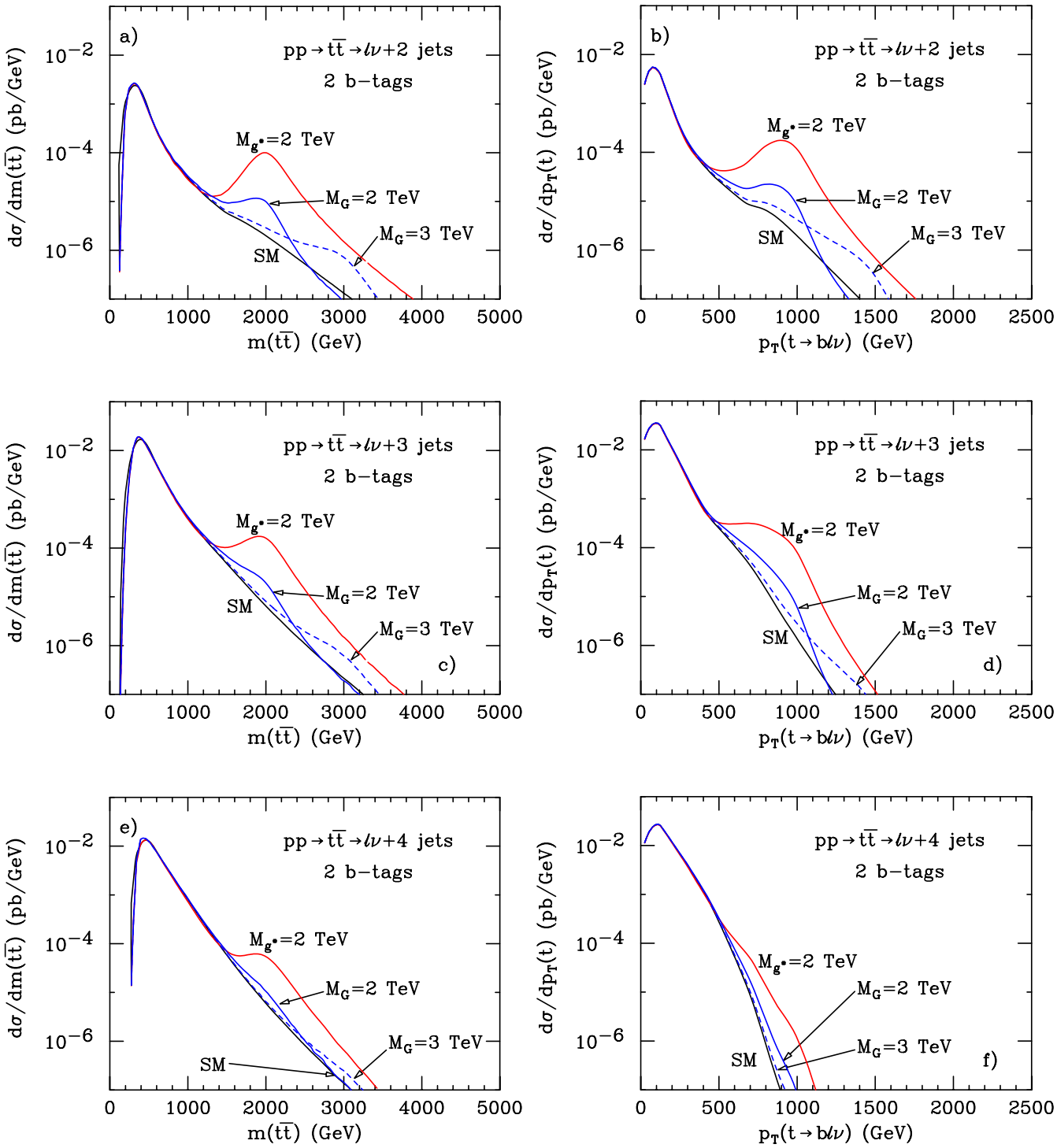

FIG. 3 (color online). The LO $pp \to t\bar{t} \to \ell\nu + n$ jets, $n = 2, 3, 4$, differential cross section at the LHC as a function of the reconstructed $t\bar{t}$ invariant mass, and the reconstructed p_T of the semileptonically decaying top quark. Two of the jets are assumed to be b-tagged. Shown are the cross sections for two, three, and four jets in the final state in the SM (black lines) and for two types of KK gluon excitations (see text). The cuts imposed are listed in Eqs. (4)–(7). In addition an isolation cut [see Eq. (8)] with $R_{\text{min}} = 0.4$ is imposed and jets with $\Delta R < 0.4$ are merged.

events [13,14]. The jet invariant mass cut will be discussed in more detail in Sec. IV. Alternatively, one can pursue a strategy similar to that discussed in Refs. [37,38]. $t\bar{t} \to \ell\nu + 3$ jet events at high energies originate either from the merging of the two light quark jets from $W \to q\bar{q}'$, or from the merging of one light quark jet with a b-jet.

SM $t\bar{t}$ production at the LHC is dominated by gluon fusion and the t-channel top quark exchange diagram is

playing an important role in this process. As a result, top quarks tend to be produced with a fairly large rapidity, i.e. with a large $t\bar{t}$ invariant mass but a relatively small top quark p_T. The steeply falling $p_T(t)$ distribution [see Fig. 2(b)] reflects this behavior. New physics particles decaying into $t\bar{t}$, $X \to t\bar{t}$, manifest themselves as s-channel resonances, leading to a Jacobian peak in the top quark transverse momentum distribution which peaks at $M_X/2$, where M_X is the X mass. The relatively larger impact the $t\bar{t} \to \ell\nu + 2, 3$ jet final states have on the SM $p_T(t)$ distribution, therefore, should carry over to the $m(t\bar{t})$ distribution in the vicinity of the X resonance, i.e. the X resonance should be significantly more pronounced in lepton + jets events with 2 or 3 jets. This is borne out in Fig. 3, where we show the $t\bar{t}$ invariant mass and top quark p_T distributions for the $t\bar{t} \to \ell\nu + n$ jet final states with $n = 2, 3$ in the SM (black solid lines), and for two types of KK excitations of the gluon. For comparison, we also show the differential cross sections for $n = 4$. The red curves give predictions for a KK gluon, g^*, with $M_{g^*} = 2$ TeV, vectorlike couplings to quarks and coupling strength $g_{g^*} = \sqrt{2}g_s$, where g_s is the QCD coupling constant [18,19]. The solid and dashed blue lines show the cross sections for bulk RS KK gluons, G, with $M_G = 2$ TeV and 3 TeV, respectively [13,14]. Bulk RS KK gluons have vectorlike couplings with strength $g_G = -0.2g_s$ to all quarks except the top and bottom quarks for which $g^b_{GL} = g_s$, $g^b_{GR} = -0.2g_s$, $g^t_{GL} = g_s$ and $g^t_{GR} = 4g_s$. The width of the KK gluons is taken to be $\Gamma_{g^*,G} = 0.17M_{g^*,G}$. They do not couple to gluons at LO. It is obvious that the $\ell\nu + 2$ jet and $\ell\nu + 3$ jet final states offer a much better chance to discover such $t\bar{t}$ resonances, especially if the mass of the resonance is larger than 2 TeV. Qualitatively similar results are obtained for other types of $t\bar{t}$ resonances. However, if they couple weakly to top quarks, such as Z' bosons appearing in little Higgs or topcolor models, their significance may be very much reduced.

As discussed in more detail in Sec. II C, the value of ϵ_b used in this section may well be too optimistic for very energetic top quarks [6,19]. Although the b-tagging efficiency degrades with increasing $p_T(t)$ and $t\bar{t}$ invariant masses, it equally affects the cross section of the 2 jet, 3 jet, and 4 jet final states. The main result of this section, namely, that the $\ell\nu + 2$ jets and $\ell\nu + 3$ jets final states may significantly increase the $t\bar{t}$ cross section for very energetic top quarks, therefore does not depend on the value of ϵ_b used.

B. NLO QCD corrections to the lepton + jets final state at high energies

So far, our calculations have been limited to lowest order in perturbation theory. Since QCD corrections to top pair production are known to be significant, we now study how NLO QCD corrections affect the lepton + jets final state topologies. QCD corrections may change the normalization and/or the shape of distributions. In addition, hard QCD bremsstrahlung may produce additional isolated jets which complicate the reconstruction of the $t\bar{t}$ invariant mass and the top quark transverse momentum distribution. QCD corrections apply to both the top production and decay processes; interference between the two is negligible in the narrow width approximation, which we employ. For $R_{\min} = 0.4$ and $p_T(t) > 500$ GeV, most extra jets originate from production-stage radiation, i.e. from QCD corrections for $t\bar{t}$ production. Jets coming from decay-stage radiation, i.e. from QCD corrections to $t \to b\ell\nu$ and $t \to bq\bar{q}'$, rarely lead to additional isolated jets in this region. As in the case of LO hadronic top decay, this is due to the large Lorentz boost. For $p_T(t) < 500$ GeV, decay-stage radiation will slightly modify the relative fraction of 2, 3, and 4 jet final state events. For a more quantitative statement, and to investigate what role decay-stage radiation plays for $p_T < 500$ GeV, the NLO QCD corrections to $t\bar{t}$ production including top quark decays are needed, which presently do not exist. Decay-stage radiation therefore is not discussed in the following.

We first investigate how NLO QCD corrections to $t\bar{t}$ production modify the shape and normalization of the $m(t\bar{t})$, $p_T(t \to b\ell\nu)$, and $p_T(t \to bjj)$ distributions for a given number of $t\bar{t}$ decay jets. This assumes that the jets from the hadronic top decay have been correctly identified, for example, by imposing an invariant mass cut on one or several jets. Subsequently, we will then discuss how QCD corrections affect these distributions for fixed observed jet multiplicities.

The NLO QCD corrections to $t\bar{t}$ production have been known for more than 15 years [39]. A more recent calculation [40] includes top quark decays and spin correlations. The NLO QCD corrections to $t\bar{t}$ production have been interfaced with the HERWIG shower Monte Carlo [41] in the program MC@NLO [42]. This produces a realistic $t\bar{t}$ transverse momentum distribution. Furthermore, MC@NLO includes top quark decay [43] and thus makes it possible to include acceptance cuts in the calculation. Using MC@NLO to compute the $t\bar{t}$ cross section including QCD corrections, we show the NLO to LO cross section ratio (k-factor) for $pp \to t\bar{t} \to \ell\nu + n$ jets, $n = 2, 3, 4$, as a function of the reconstructed $t\bar{t}$ invariant mass in Fig. 4 (solid histograms). Here, and in all other figures in this section, n is the number of jets resulting from the decay of the $t\bar{t}$ pair, *not* the number of jets in the event. Furthermore, we call the cross section obtained with MC@NLO the "NLO" cross section, although this is, strictly speaking, not correct: MC@NLO does take into account multiple gluon radiation in the leading log approximation.

For 3 jet and 4 jet final states, Fig. 4 shows that the k-factor increases slowly with $m(t\bar{t})$. In the 2 jet case, it rises at low invariant masses, and then decreases somewhat for $m(t\bar{t}) > 1$ TeV. We also show the fraction of NLO $pp \to t\bar{t} \to \ell\nu + n$ jet events with $p_T(t\bar{t}) > 100$ GeV in

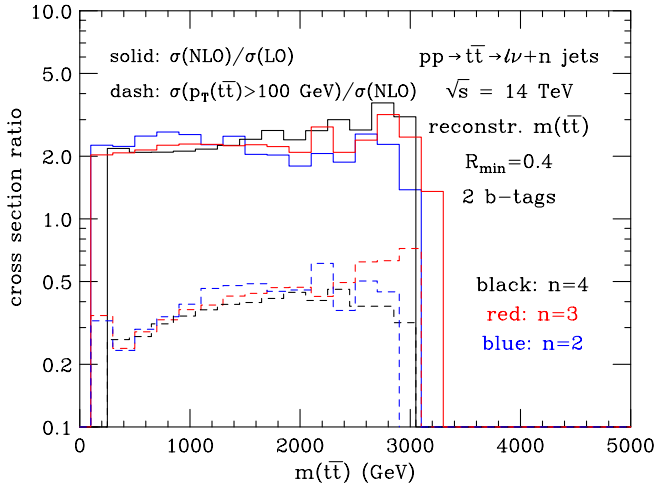

FIG. 4 (color online). The NLO to LO $pp \to t\bar{t} \to \ell\nu + n$ jets cross section ratio (solid histograms) at the LHC as a function of the reconstructed $t\bar{t}$ invariant mass. Here, n is the number of $t\bar{t}$ decay jets. The dashed histograms display the fraction of the NLO $pp \to t\bar{t} \to \ell\nu + n$ jets events for which $p_T(t\bar{t}) > 100$ GeV. Shown are the cross section ratios for two (blue), three (red), and four (black) $t\bar{t}$ decay jets. Two of the jets are assumed to be b-tagged. The cuts imposed are listed in Eqs. (4)–(7). In addition an isolation cut [see Eq. (8)] with $R_{\min} = 0.4$ is imposed. $t\bar{t}$ decay jets with a separation $\Delta R < 0.4$ have been merged.

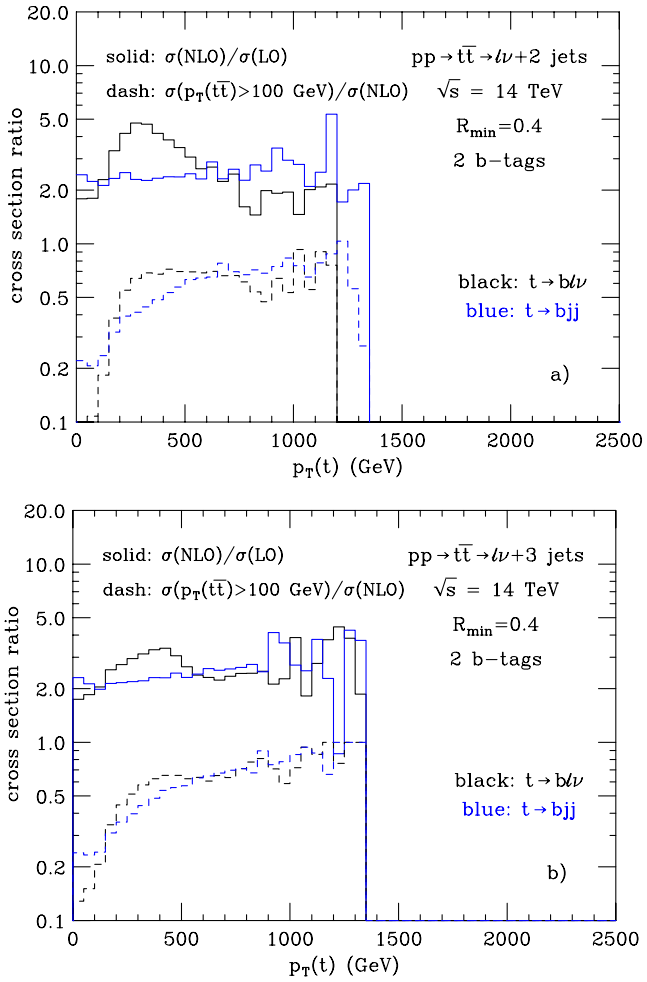

FIG. 5 (color online). The NLO to LO cross section ratio (solid histograms) for $pp \to t\bar{t} \to \ell\nu + n$ jets at the LHC as a function of the $t \to b\ell\nu$ (black) and $t \to bjj$ (blue) transverse momentum for (a) two ($n = 2$) and (b) three ($n = 3$) $t\bar{t}$ decay jets. The dashed histograms display the fraction of the NLO $pp \to t\bar{t} \to \ell\nu + n$ jet events ($n = 2, 3$) for which $p_T(t\bar{t}) > 100$ GeV. Two of the jets are assumed to be b-tagged. The cuts imposed are listed in Eqs. (4)–(7). In addition an isolation cut [see Eq. (8)] with $R_{\min} = 0.4$ is imposed. $t\bar{t}$ decay jets with a separation $\Delta R < 0.4$ have been merged.

Fig. 4 (dashed histograms). The fraction increases from about 25% at low invariant mass to 40%–50% at $m(t\bar{t}) \geq 2$ TeV.

Figures 5 and 6 show the k-factor and the fraction of events with $p_T(t\bar{t}) > 100$ GeV (at NLO) as a function of the p_T of the semileptonically and the hadronically decaying top quark. As mentioned before, at LO the p_T distributions of the two top quarks in $t\bar{t}$ production are identical. This is no longer the case at NLO. Figures 5 and 6 show that the differential k-factors can be quite different for $t \to b\ell\nu$ and $t \to bjj$. The difference is most pronounced in the 2 jet final state [Fig. 5(a)]. In the region $p_T(t \to bjj) > 700$ GeV most $t \to bjj$ jets merge into a single jet. This favors a kinematical configuration where $p_T(t \to b\ell\nu) < p_T(t \to bjj)$, i.e. where the QCD jet(s) and the semileptonically decaying top quark are in the same hemisphere. As a result, the fraction of events with $p_T(t\bar{t}) > 100$ GeV for $p_T(t \to bjj) > 700$ GeV is larger than that for $t \to b\ell\nu$ in the same range. In turn, the fraction of events with $p_T(t\bar{t}) > 100$ GeV for $p_T(t \to bjj) < 700$ GeV is smaller than that for $t \to b\ell\nu$. Below a p_T of about 250 GeV, a new effect comes into play. If $p_T(t\bar{t}) > 100$ GeV and $p_T(t \to b\ell\nu)$ is small, the hadronically decaying top quark has to carry a transverse momentum of $\mathcal{O}(100$ GeV). This makes it likely that one of the light quark jets originating from $t \to bjj$ satisfies the jet acceptance cuts. On the other hand, the top quark transverse momentum is not high enough for jet merging. For small $p_T(t \to b\ell\nu)$, events with a large transverse momentum of the $t\bar{t}$ system thus are very unlikely (black dashed histogram).

The evolution of the event fraction with $p_T(t\bar{t}) > 100$ GeV as a function of $p_T(t \to b\ell\nu)$ is directly reflected in the corresponding k-factor. The preference for events with $p_T(t \to b\ell\nu) < p_T(t \to bjj)$ for $p_T(t \to bjj) > 700$ GeV leads to a very large k-factor for 250 GeV $< p_T(t \to b\ell\nu) < 700$ GeV. The suppression of events with high $t\bar{t}$ transverse momentum at small $p_T(t \to b\ell\nu)$ then causes the k-factor to sharply drop for $p_T(t \to b\ell\nu) <$ 250 GeV (solid black histogram). While the k-factor varies significantly with $p_T(t \to b\ell\nu)$, it is essentially uniform for $p_T(t \to bjj) < 800$ GeV.

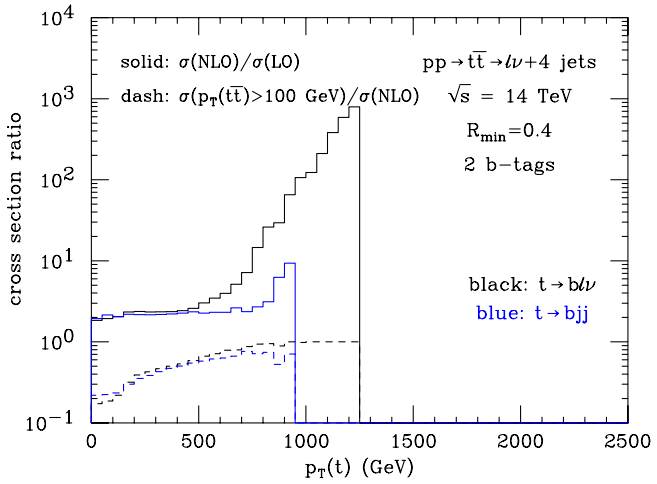

FIG. 6 (color online). The NLO to LO $pp \to t\bar{t} \to \ell\nu + 4$ jets cross section ratio (solid histograms) at the LHC as a function of the $t \to b\ell\nu$ (black) and $t \to bjj$ (blue) transverse momentum. The dashed histograms display the fraction of the NLO $pp \to t\bar{t} \to \ell\nu + 4$ jet events for which $p_T(t\bar{t}) > 100$ GeV. The number of jets here refers to $t\bar{t}$ decay jets, and we assume that two of them are b-tagged. The cuts imposed are listed in Eqs. (4)–(7). In addition an isolation cut [see Eq. (8)] with $R_{\min} = 0.4$ is imposed. $t\bar{t}$ decay jets with a separation $\Delta R < 0.4$ have been merged.

The k-factor and the fraction of events with $p_T(t\bar{t}) > 100$ GeV for the 3 jet and the 2 jet final state show the same qualitative behavior. In the 3 jet final state, an even larger fraction of events has a $t\bar{t}$ transverse momentum larger than 100 GeV, especially for very large top quark p_T [dashed histograms in Fig. 5(b)]. At low $p_T(t \to b\ell\nu)$, the suppression of events with high $p_T(t\bar{t})$ is less pronounced than in the 2 jet final state. Consequently, the variation of the k-factor with $p_T(t \to b\ell\nu)$ is smaller than for $t\bar{t} \to \ell\nu +$ 2 jets. The k-factor slowly increases with $p_T(t \to bjj)$ over the entire p_T range.

In the 4 jet final state, the k-factor is uniform for $p_T(t \to b\ell\nu) < 500$ GeV (see Fig. 6). For higher values, it becomes very large. For very large $p_T(t \to b\ell\nu)$, the $t\bar{t}$ transverse momentum of essentially all events exceeds 100 GeV (dashed black histogram in Fig. 6). In contrast, the k-factor stays uniform up to transverse momenta of about 800 GeV for the hadronically decaying top quark. The extremely large k-factor for $p_T(t \to b\ell\nu) > 500$ GeV is a consequence of the separation cut which affects $t \to bjj$ much more than $t \to b\ell\nu$ at large p_T. As a result, events which contain one or more hard QCD jets in the hemisphere opposite to that of the $t \to b\ell\nu$ decay products are kinematically favored. For the same reason, $t\bar{t}W$ and $t\bar{t}Z$ production becomes important for large values of $p_T(t \to b\ell\nu)$ [44].

NLO QCD corrections mostly change the normalization of the $m(t\bar{t})$ and $p_T(t \to bjj)$ distributions. For these distributions, the cross section hierarchy for 2, 3, and 4 $t\bar{t}$ decay jets shown in Fig. 2 remains unchanged. With the extremely large k-factor for the 4 jet final state, this is not obvious for the $p_T(t \to b\ell\nu)$ distribution. Figure 7 shows that for $p_T(t \to b\ell\nu) > 600$ GeV [$p_T(t \to b\ell\nu) > 900$ GeV] the cross section for the final state with 3 (2) jets from $t\bar{t}$ decays still exceeds that of the channel with 4 $t\bar{t}$ decay jets when NLO QCD corrections are taken into account.

In phase space regions where most top pair events have a large transverse momentum, the NLO $t\bar{t}$ cross section is dominated by the tree-level process $pp \to t\bar{t}j$. As a result, the NLO cross section depends significantly on the choice of the factorization and renormalization scale in these regions.

So far we have classified events by the number of $t\bar{t}$ decay jets. The number of extra jets from QCD radiation in $t\bar{t}$ production was not specified. At large top quark transverse momentum, we found that most events have $p_T(t\bar{t}) > 100$ GeV and thus have one or more extra hard jets. These extra jets introduce a combinatorial background. Considering final states with a fixed jet multiplicity of 2, 3, or 4 jets, and requiring that the invariant mass of the jet(s) excluding the b-jet with the smaller separation from the charged lepton is consistent with m_t, is expected to suppress hard extra QCD jets in the event, and thus the combinatorial background. As we shall demonstrate in Secs. III and IV, such a cut will also be helpful in reducing the background to an acceptable level. If no hard QCD jets are produced, the $t\bar{t}$ transverse momentum will be small. A rough estimate of the QCD corrections to $pp \to t\bar{t} \to \ell\nu + n$ jets with no hard extra QCD jets can be obtained from the k-factor for events with $p_T(t\bar{t}) < 100$ GeV, $k_{<100}$.

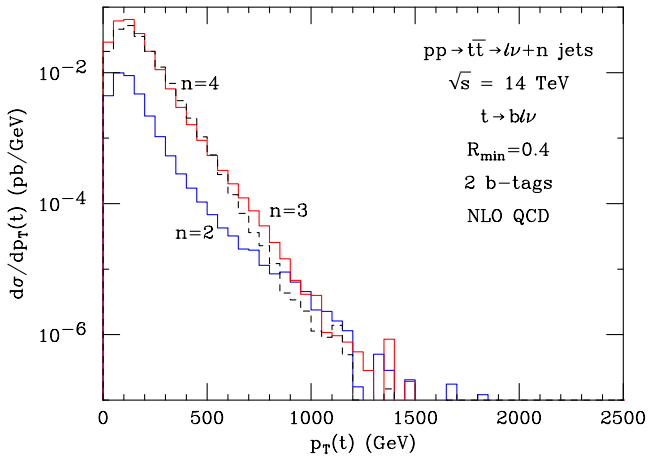

FIG. 7 (color online). The NLO $pp \to t\bar{t} \to \ell\nu + n$ jets cross section at the LHC as a function of the $t \to b\ell\nu$ transverse momentum. n is the number of $t\bar{t}$ decay jets in the event, and two of these jets are assumed to be b-tagged. The solid blue and red histograms show the cross sections for $n = 2$ and $n = 3$, respectively. The dashed histogram represents the $n = 4$ cross section. The cuts imposed are listed in Eqs. (4)–(7). In addition an isolation cut [see Eq. (8)] with $R_{\min} = 0.4$ is imposed. $t\bar{t}$ decay jets with a separation $\Delta R < 0.4$ have been merged.

$k_{<100}$ can be calculated from the inclusive k-factor, $k_{\rm incl}$, and the ratio of the NLO cross section with $p_T(t\bar{t}) > 100$ GeV and the inclusive NLO rate, r,

$$k_{<100} = k_{\rm incl}(1 - r), \tag{10}$$

which are both shown in Figs. 4–6. The $k_{<100}$ distributions as a function of $m(t\bar{t})$, $p_T(t \to b\ell\nu)$, and $p_T(t \to bjj)$ are qualitatively very similar. $k_{<100}$ is found to decrease smoothly from $k_{<100} \approx 1.5$–1.7 at low $m(t\bar{t})$ and $p_T(t)$ to $k_{<100} \approx 0.7$–0.8 at large values. QCD corrections for top quark pairs with small transverse momentum thus are smaller than in the inclusive case, and result in somewhat steeper falling $m(t\bar{t})$ and $p_T(t)$ distributions than at LO.

Quantitative results of course depend on the jet p_T threshold considered; for a lower (higher) threshold of $p_T(t\bar{t})$, a smaller (larger) k-factor is found. More detailed simulations, which are beyond the scope of our paper, are required to develop a better understanding how QCD corrections affect the $m(t\bar{t})$ and $p_T(t)$ distributions for fixed jet multiplicities when an invariant mass cut on one or more jets is imposed.

C. b-tagging for very energetic top quarks

So far, in our analysis, we have assumed that both b-quarks in $pp \to t\bar{t} \to \ell\nu b\bar{b}q\bar{q}'$ are tagged with an efficiency of $\epsilon_b = 60\%$ each. However, for very energetic top quarks, the b-tagging efficiency is expected to degrade [14]. This is easy to understand. The energy of the b-quark in $t \to b\ell\nu$ or $t \to bjj$ is on average about $1/3$ of that of the parent top quark. The higher the energy of the b-quark, the more collimated the b decay products are. Because of the finite angular resolution of the LHC detectors, this will increase the uncertainty in the position of the reconstructed secondary vertex, and thus decrease the tagging efficiency. In hadronic top decays where two or more jets merge, the overlapping of the b-jet with one or several light quark jets may additionally complicate the reconstruction of the secondary vertex which is expected to result in a further decrease in ϵ_b. The increased decay length of very energetic b-quarks, which makes it easier to tag b-quarks, is not expected to compensate these effects.

Although detailed simulations of b-tagging for very energetic top quarks do not exist yet, preliminary studies [6,19] indicate that ϵ_b may decrease by a factor 2–3 in the TeV region. Simultaneously, the probability for misidentifying a light quark, gluon, or c-jet as a b-jet may increase by up to a factor 3.

A decrease of ϵ_b by a factor 2–3 in the high-energy regime results in a reduction of the observable $t\bar{t}$ cross section by up to a factor 10. However, the efficiency for tagging only one b-quark in a $t\bar{t}$ event,

$$\epsilon(1\ \text{tag}) = 2\epsilon_b(1 - \epsilon_b), \tag{11}$$

is much less sensitive to ϵ_b than $\epsilon(2\ \text{tags}) = \epsilon_b^2$. For $\epsilon_b = 0.2$–0.6, $\epsilon(1\ \text{tag}) = 0.32$–$0.48$, i.e. it varies by less than a factor of 2. For small ϵ_b, the cross section of the lepton + jets final state with one b-tag is much larger than that for two b-tags. For example, for $\epsilon_b = 0.2$, $\epsilon(1\ \text{tag})/\epsilon(2\ \text{tags}) = 8$. This, and the relative stability of the one tag cross section to variations of $\epsilon(b)$, make the lepton + jets final state with one b-tag an attractive channel in the search for resonances in the $t\bar{t}$ channel.

The increase in rate in the lepton + jets channel with one b-tag comes at the price of a potentially much larger background. The background for both one and two b-tags in the lepton + jets channel will be examined in detail in Sec. III.

D. The dilepton + jets and all-hadronic final states

Our discussion, so far, has been focused on the lepton + jets final state. In this section we investigate whether the $t\bar{t}$ dilepton and all-hadronic final states can significantly increase the range in $m(t\bar{t})$ and/or $p_T(t)$ which can be accessed at the LHC.

In the dilepton channel, $pp \to t\bar{t} \to \ell^{\pm}\nu_\ell\ell'^{\mp}\nu_{\ell'}b\bar{b}$ ($\ell, \ell' = e, \mu$), one requires two isolated leptons with opposite charge, two jets with at least one b-tag, and a substantial amount of $\not{p}_T$. The main disadvantages of the dilepton final state are its small branching ratio of $\approx 4.7\%$, and the two neutrinos in the final state which make it impossible to reconstruct the $t\bar{t}$ invariant mass or the p_T of the individual top quarks. However, the $\ell\ell'\not{p}_T + 2$ jets final state is much less sensitive to the isolation cut at high energies than $pp \to t\bar{t} \to \ell\nu + 4$ jets which makes it worthwhile to investigate. The main background in this channel comes from Z + jets and $WWb\bar{b}$ production [28].

Since the $t\bar{t}$ invariant mass cannot be reconstructed in the dilepton final state, one has to use the $\ell\ell' b\bar{b}$ cluster transverse mass,

$$m_{Tcl}^2 = (\sqrt{p_T^2(\ell\ell' b\bar{b}) + m^2(\ell\ell' b\bar{b})} + \not{p}_T)^2 - (\vec{p}_T(\ell\ell' b\bar{b}) + \vec{\not{p}}_T)^2, \tag{12}$$

where $p_T(\ell\ell' b\bar{b})$ and $m(\ell\ell' b\bar{b})$ are the transverse momentum and invariant mass of the $\ell\ell' b\bar{b}$ system, respectively, to search for resonances. The cluster transverse mass distribution in the SM and for the KK gluon states discussed in Sec. II A is shown in Fig. 8. We require at least one b-quark to be tagged and impose the same cuts as in Secs. II A and II B. The cluster transverse mass distribution is seen to fall much more rapidly than that of the $t\bar{t}$ invariant mass. The dilepton final state therefore will not be competitive with the lepton + jets final state when searching for $t\bar{t}$ resonances, and we will not discuss it further in this paper.

The all-hadronic final state, $t\bar{t} \to bq_1\bar{q}_2\bar{b}q_3\bar{q}_4$ has the largest branching ratio ($\approx 46\%$) but also the largest background. In order to reduce the QCD multijet background to an acceptable level, two b-tags have to be required. Imposing a standard $R_{\rm min} = 0.4$ isolation cut on the

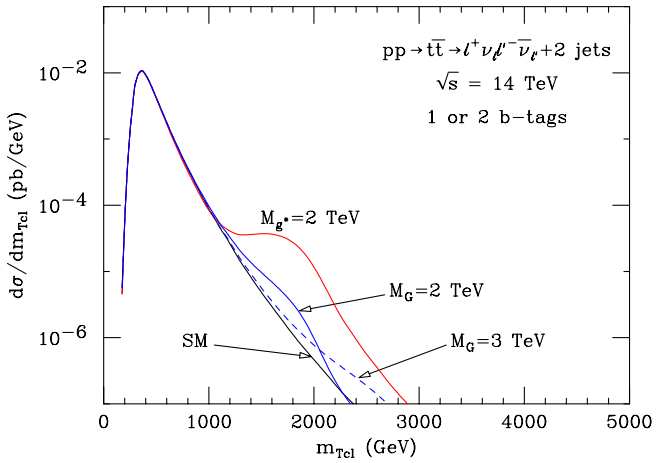

FIG. 8 (color online). The LO $pp \to t\bar{t} \to \ell^{\pm}\nu_{\ell}\ell'^{\mp}\nu_{\ell'}b\bar{b}$ differential cross section at the LHC as a function of the cluster transverse mass [see Eq. (12)]. At least one of the b-quarks is assumed to be tagged. Shown are the cross sections in the SM (black lines) and for two types of KK gluon excitations (see Sec. II A). The cuts imposed are listed in Eqs. (4)–(7). In addition an isolation cut [see Eq. (8)] with $R_{\min} = 0.4$ is imposed.

b-jets and the four light quark jets, the main background originates from QCD $b\bar{b} + 4$ jet production, which is approximately 1 order of magnitude larger than the signal [27,28].

As in the lepton + jets mode, the isolation cut strongly reduces the observable cross section in the all-hadronic final state for very energetic top quarks. In this region of phase space, some or all of the jets originating from top quark decay may merge, i.e. the LO $t\bar{t}$ signal is spread out over the $b\bar{b} + n$ jets final states with $0 \le n \le 4$. The QCD background for $0 \le n \le 3$ is expected to be of the same size or larger than that in the $b\bar{b} + 4$ jet channel.

The large background makes it difficult to utilize the all-hadronic final state in a search for $t\bar{t}$ resonances. In the following, we therefore concentrate on the lepton + jets final state with one or two b-tags.

III. BACKGROUND CALCULATIONS FOR THE LEPTON + JETS FINAL STATE

In Sec. II, we have shown that extending the search criteria for the lepton + jets final state to include topologies with less than 4 jets and/or one b-tag may considerably increase the number of $t\bar{t}$ candidate events. These final states, however, will be useful in a search for $t\bar{t}$ resonances only if the backgrounds are sufficiently small. It is well known [27,28,45] that the background is indeed small in the 4 jet case with two b-tags. Here we calculate the backgrounds contributing to the 2 jet and 3 jet final states and compare it with that obtained in the 4 jet case. We consider final states with one or two b-tags. Backgrounds where one or two light quark, gluon, or c-quark jets are misidentified as a b-jet are included in our calculation.

For a realistic estimate of the backgrounds in the $m(t\bar{t})$ and $p_T(t)$ distributions, parametrizations of ϵ_b and the misidentification probabilities of light jets ($P_{q,g\to b} = P_{j\to b}$, $q = u, d, s$) and charm quarks ($P_{c\to b}$) as b-jets are needed as a function of the b-quark energy or p_T. Currently, these do not exist. Except for low energies, ϵ_b is known only for a few selected values of $m(t\bar{t})$ [6,19] which is insufficient for calculating the backgrounds as a function of the $t\bar{t}$ invariant mass, or the top quark transverse momentum. In the following, we therefore present numerical results using $\epsilon_b = 0.6$ and misidentification probabilities of $P_{j\to b} = 1/100$ and $P_{c\to b} = 1/10$ [27,28]. These values are appropriate for $m(t\bar{t}) < 1$ TeV and top quark transverse momenta less than a few hundred GeV. Since the b-tagging efficiency may well be considerably lower, and the light jet mistagging probabilities significantly higher, for very energetic top quarks [6,19], we comment wherever appropriate on how our results change if $P_{j\to b}$ is increased by a factor 3 and the b-tagging efficiency, ϵ_b, is decreased by a factor 3.

The main background processes contributing to the $\ell\nu + n$ jet final states with $n = 2, 3, 4$ are $Wb\bar{b} + m$ jets, $(Wb + W\bar{b})j + m$ jets, and $Wjj + m$ jets production, $(t\bar{b} + \bar{t}b) + m$ jets, $(t + \bar{t})j + m$ jets production with $t \to b\ell\nu$, and Wbt, Wt, and Wjt production with $t \to bjj$. For each process, $m = 0, 1, 2$ and j represents a light quark or gluon jet, or a c-jet. Wt production only contributes to the 2 jet and 3 jet final states. The $(Wb + W\bar{b})j + m$ jets [$(t + \bar{t})j + m$ jets] background originates from $Wb\bar{b}j + m$ jets [$(t\bar{b} + \bar{t}b) + m$ jets] production where one of the b-quarks is not detected. We calculate these processes in the b-quark structure function approximation. We have verified that, for $m = 0$, the differential cross sections for $pp \to Wbj$ [$(t + \bar{t})j$] and $pp \to Wb\bar{b}j$ [$(t\bar{b} + \bar{t}b)j$] where one b-jet is not detected are very similar. For the 2 jet final state ($m = 0$), the NLO QCD corrections for all background processes except Wbt and Wjt production are known [46–52]. The background processes relevant for the 3 jet and 4 jet final states, however, are only known at LO. We therefore calculate all background cross sections consistently at LO, and comment wherever appropriate how NLO QCD corrections modify our results. To calculate $pp \to Wb\bar{b} + m$ jets and $pp \to Wjj + m$ jets we use ALPGEN [33]. All other background processes are calculated using MADEVENT [53].

$b\bar{b} + m$ jets production where one b-quark decays semileptonically also contributes to the background. Once a lepton isolation cut has been imposed, this background is known to be small for standard lepton + jets cuts [45]. For $b\bar{b} + m$ jets events to mimic a $t\bar{t}$ production with very energetic top quarks, the b-quarks also have to be very energetic. This will make the lepton isolation cut even

more efficient. We therefore ignore the $b\bar{b} + m$ jets background here.

$Wjj + m$ jets production in ALPGEN includes c-jets in the final state. Since $P_{c\to b}$ is considerably larger than $P_{q,g\to b}$, this underestimates the background from $W +$ charm production. However, the cross section of $W +$ charm final states is only a tiny fraction of the full $Wjj + m$ jets rate, resulting in an error which is much smaller than the uncertainty on the background from other sources. One can also estimate the $W +$ charm cross section from that of $pp \to Wb\bar{b} + m$ jets and $pp \to (Wb + W\bar{b}) + m$ jets. For the phase space cuts imposed, quark mass effects are irrelevant. Using the values of $P_{c\to b}$ given in Refs. [6,19,27], we find that the $(Wc + W\bar{c})j + m$ jets $[Wc\bar{c} + m$ jets] cross section is a factor 2–10 (5–100) smaller than the $(Wb + W\bar{b})j + m$ jets $[Wb\bar{b} + m$ jets] rate for the p_T and invariant mass range considered here.

In the following we impose the standard acceptance cuts of Eqs. (4)–(8) with $R_{\min} = 0.4$ and reconstruct the $t\bar{t}$ invariant mass using the procedure described in Sec. II A. The reconstruction of $p_T(t \to b\ell\nu)$ depends on the number of b-tags and is discussed in more detail below. For the background processes, the $m(t\bar{t})$ distribution is replaced by the reconstructed $Wb\bar{b} + m$ jets and $Wbj + m$ jets invariant mass distribution. The renormalization and factorization scales, μ_r and μ_f, of background processes involving top quarks are set to m_t; for all other background processes we choose the W mass. Since our calculations are performed at tree level, the cross section of many background processes exhibits a considerable scale dependence. However, uncertainties on the current b-tagging efficiencies and the light jet mistag probability at high energies introduce an even larger uncertainty. Our choice of μ_r and μ_f leads to a rather conservative estimate of the background cross sections; other (reasonable) choices such as $\mu_r^2 = \mu_f^2 = M_W^2 + \sum_i p_T(j_i)^2$, where i runs over all jets, lead to smaller cross sections, especially at high energies.

A. Background for lepton + jets events with two b-tags

The differential cross section of the SM $t\bar{t} \to \ell\nu + 2$ jets signal and the combined background from the processes discussed above as a function of the reconstructed $m(t\bar{t})$ and $p_T(t \to b\ell\nu)$ are shown in Fig. 9. To reconstruct $p_T(t \to b\ell\nu)$ for signal and background $\ell\nu + n$ jet final states with two b-tags, we use the method discussed in Sec. II A. Imposing the standard cuts of Eqs. (4)–(8) with $R_{\min} = 0.4$, signal and background are seen to be about equal. Only for $m(t\bar{t}) > 2.5$ TeV and $p_T(t) > 1.2$ TeV does the background dominate. The main background source is $pp \to Wb\bar{b}$, except at very high $m(t\bar{t})$ and $p_T(t)$ where Wbt production dominates.

The signal to background ratio can be significantly improved by imposing a cut

$$|m_T(b_{\min}\ell) - m_t| < 20 \text{ GeV} \tag{13}$$

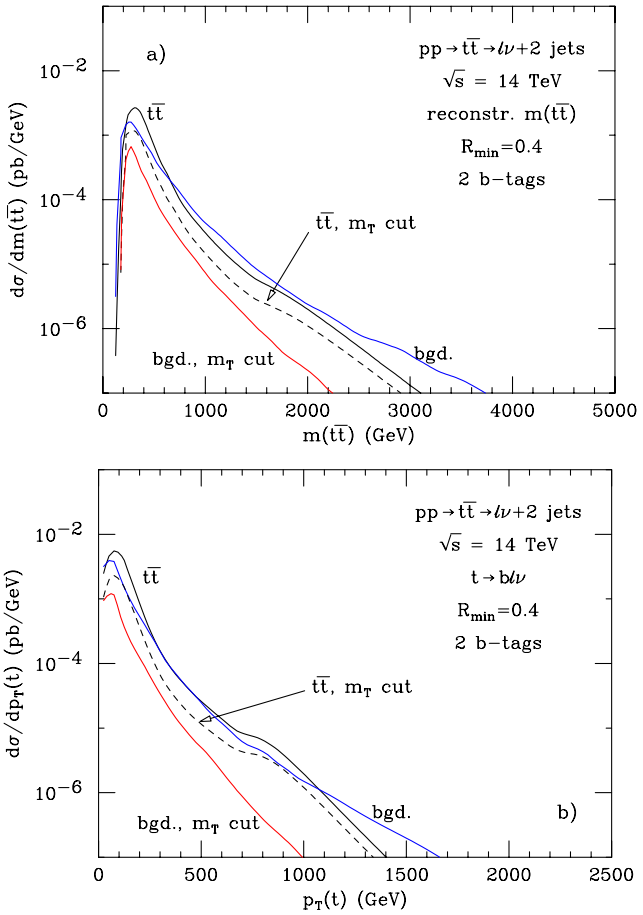

FIG. 9 (color online). The LO differential cross section of the SM $t\bar{t} \to \ell\nu + 2$ jets signal and the combined background as a function of (a) the reconstructed $t\bar{t}$ invariant mass and (b) the $t \to b\ell\nu$ transverse momentum at the LHC. The two jets are assumed to be b-tagged. The black and blue curves show the signal and background, respectively, imposing standard cuts [Eqs. (4)–(8)] with $R_{\min} = 0.4$. The dashed and red curves show signal and background if in addition a cluster transverse mass cut is imposed on the $b\ell\nu$ system [see Eq. (14)].

on the cluster transverse mass, m_T, of the $b\ell\nu$ system which is defined by

$$m_T^2(b_{\min}\ell) = (\sqrt{p_T^2(b_{\min}\ell) + m^2(b_{\min}\ell)} + \not{p}_T)^2 - (\vec{p}_T(b_{\min}\ell) + \vec{\not{p}}_T)^2, \tag{14}$$

where $p_T(b_{\min}\ell)$ and $m(b_{\min}\ell)$ are the transverse momentum and invariant mass of the $b_{\min}\ell$ system, respectively, and $b_{\min}$ is the b- or $\bar{b}$-quark which has the smaller separation from the charged lepton. m_T sharply peaks at the top mass. The cluster transverse mass reduces the signal by about a factor 2 (1.5) at small (large) invariant masses and p_T's (dashed curves). The background, on the other hand, decreases by a factor 5–10. At large $m(t\bar{t})$ and $p_T(t \to b\ell\nu)$, $(t\bar{b} + \bar{t}b)$ production is the dominant contribution to the background after the m_T cut has been imposed. At

low energies, $pp \to Wb\bar{b}$ is still the largest background source.

The $t\bar{t}$ signal in the $\ell\nu + 2$ jets final state with two b-tags necessarily requires a small transverse momentum of the $t\bar{t}$ system. As discussed in Sec. II B, the NLO $m(t\bar{t})$ and $p_T(t)$ distributions fall somewhat faster than those at LO if the transverse momentum of the $t\bar{t}$ system is small. It is important to know whether the corresponding distributions of the dominant background processes, $pp \to Wb\bar{b}$ and $pp \to (t\bar{b} + \bar{t}b)$, show the same behavior, or whether QCD corrections worsen the signal to background ratio. Calculating the NLO corrections to these processes using the program MCFM [54] and imposing a veto on additional hard jets, we find that they have a similar effect on the signal and the background distributions. QCD corrections thus will not change the signal to background ratio significantly.

In Fig. 10, we show the $t\bar{t}$ signal and the combined background for the 3 jet final state. Imposing the standard cuts of Eqs. (4)–(8) only, the background is small at low values of $m(t\bar{t})$ and $p_T(t \to b\ell\nu)$ but dominates over the signal in the TeV region. Imposing a m_T cut [see Eq. (13)] improves the situation. However, the background is still larger than the signal for $m(t\bar{t}) > 1.8$ TeV and $p_T(t) > 1$ TeV. To further improve the signal to background ratio one can impose an invariant mass cut on the $b_{\max}j$ system,

$$|m(b_{\max}j) - m_t| < 20 \text{ GeV}, \tag{15}$$

where j is the nontagged jet and $b_{\max}$ is the b-quark with the larger separation from the charged lepton. The invariant mass resolution for jet systems with a mass near m_t is approximately 7–10 GeV for jets with energies above 200 GeV. The invariant mass window chosen in Eq. (15) thus will capture most of the $t\bar{t}$ signal. On the other hand, it is sufficiently narrow to reject a large portion of the background. Indeed, the $m(b_{\max}j)$ cut suppresses the background by an additional factor 3–10 for $m(t\bar{t}) > 1.8$ TeV (magenta line), while it has a much smaller effect on the signal in this region (dashed blue curve). Note that the $m(b_{\max}j)$ cut does reduce the signal by up to a factor 10 at small $t\bar{t}$ invariant masses. In this region most $t\bar{t} \to \ell\nu + 3$ jets events are the result of one jet not satisfying the p_T and pseudorapidity cuts, and not of the merging of $t \to bjj$ jets. If a jet fails the acceptance cuts, the $b_{\max}j$ system usually will not be in the vicinity of the top quark mass.

Once a $m(b_{\max}j)$ cut has been imposed, the background is smaller than the signal over the entire p_T and invariant mass range of interest. The main background sources in this case are $(t\bar{b} + \bar{t}b)j$ and Wbt production. Without the $m(b_{\max}j)$ cut, the main contributions to the background in the 3 jet final state originate from $Wb\bar{b}j$ and $(t\bar{b} + \bar{t}b)j$ production.

For completeness, we show the $t\bar{t}$ invariant mass and top quark p_T distribution for the 4 jet final state in Fig. 11. Once a m_T and a

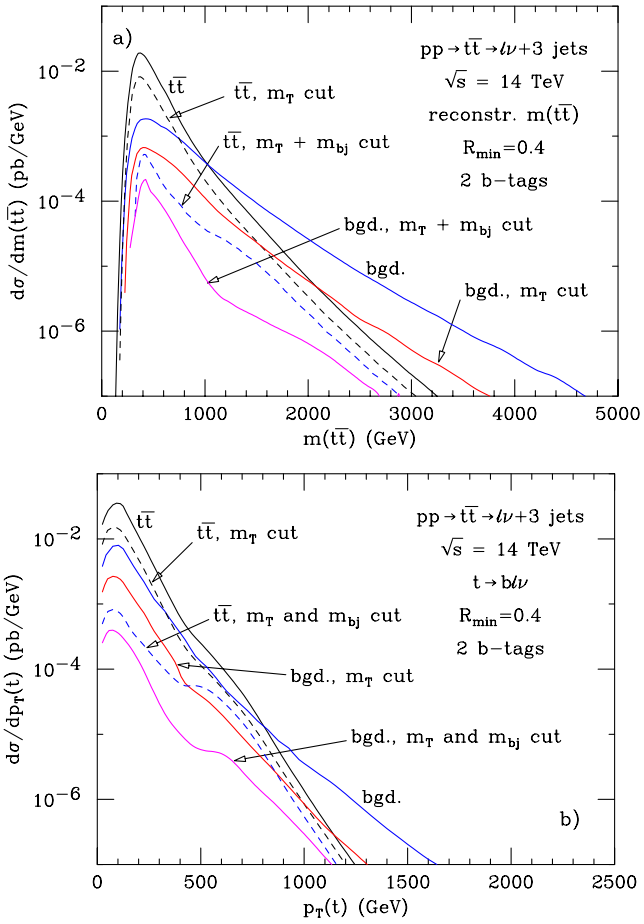

FIG. 10 (color online). The LO differential cross section of the SM $t\bar{t} \to \ell\nu + 3$ jets signal and the combined background as a function of (a) the reconstructed $t\bar{t}$ invariant mass and (b) the $t \to b\ell\nu$ transverse momentum at the LHC. Two jets are assumed to be b-tagged. The black and blue curves show the signal and background, respectively, imposing standard cuts [Eqs. (4)–(8)] with $R_{\min} = 0.4$. The dashed and red curves show signal and background if in addition a cluster transverse mass cut is imposed on the $b\ell\nu$ system [see Eq. (14)]. The blue dashed and magenta curves, finally, show signal and background if in addition the invariant mass cut of Eq. (15) is imposed.

$$|m(b_{\max}jj) - m_t| < 20 \text{ GeV}, \tag{16}$$

cut have been imposed, the background is below the signal for all top quark transverse momenta and $t\bar{t}$ invariant masses of interest. The $m(b_{\max}jj)$ cut has essentially no effect on the signal for $m(t\bar{t}) > 600$ GeV and $p_T(t) > 200$ GeV. The main background source in the 4 jet channel with (without) a $m(b_{\max}jj)$ cut is Wbt [single resonant $(t\bar{b} + \bar{t}b)jj$ and $Wb\bar{b}jj$] production. Note that we have not imposed a cut on the invariant mass of the two light quark jets, $m(jj)$. It peaks near M_W for both the signal and the Wbt, $t \to bjj$, background. Once a $m(b_{\max}jj)$ cut has been imposed, a $m(jj)$ cut thus will have little effect on the signal to background ratio.

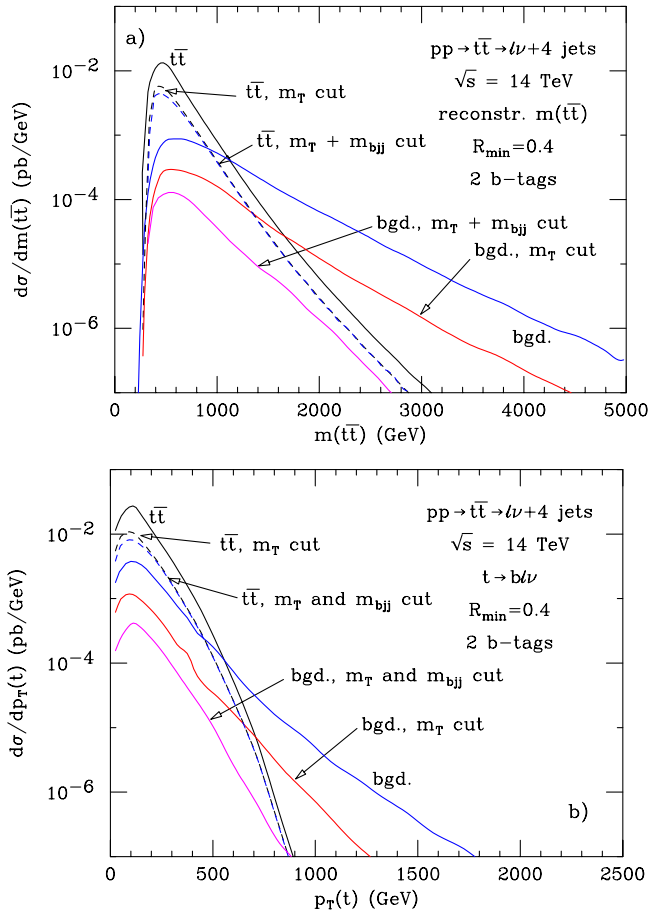

FIG. 11 (color online). The LO differential cross section of the SM $t\bar{t} \to \ell\nu + 4$ jets signal and the combined background as a function of (a) the reconstructed $t\bar{t}$ invariant mass and (b) the $t \to b\ell\nu$ transverse momentum at the LHC. Two jets are assumed to be b-tagged. The black and blue curves show the signal and background, respectively, imposing standard cuts [Eqs. (4)–(8)] with $R_{\min} = 0.4$). The dashed and red curves show signal and background if in addition a cluster transverse mass cut is imposed on the $b\ell\nu$ system [see Eq. (14)]. The blue dashed and magenta curves, finally, show signal and background if in addition the invariant mass cut of Eq. (16) is imposed.

As we have mentioned before, the b-tagging efficiency at high invariant masses and transverse momenta may be up to a factor 3 smaller, and the misidentification probability for light quark and gluon jets may be up to factor 3 larger, than at small $m(t\bar{t})$ and $p_T(t)$. If this is indeed the case, Wjj production becomes the largest background source in $pp \to t\bar{t} \to \ell\nu + 2$ jets, and exceeds the signal by about a factor 2 in the $m(t\bar{t})$ distribution, even if a m_T cut is imposed. To further improve the signal to background ratio in this channel, a cut on the invariant mass of the t-jet which originates from the $t \to bjj$ jet merging may be useful. This will be discussed in more detail in Sec. IV. In the $p_T(t)$ distribution, the background remains smaller than the signal for $p_T(t) > 700$ GeV. For the 3 jet and 4 jet final states, Wbt production remains the most important background for very energetic top quarks, and the signal is still larger than the combined background once a cluster transverse mass and $m(b_{\max} j(j))$ cut have been imposed.

B. Background for lepton + jets events with one b-tag

As discussed in Sec. II C, the cross section for $pp \to t\bar{t} \to \ell\nu + n$ jets with one b-tag may be significantly larger than that of final states with two b-tags if ϵ_b is small. In this Section, we consider the background to the lepton + jets mode with one b-tag. As before, we assume $\epsilon_b = 0.6$ and $P_{j\to b} = 1/100$ in our simulations and comment on how the signal to background ratio changes if the b-tagging efficiency decreases, and $P_{j\to b}$ increases, by a factor of 3.

In addition to final states with 2, 3, or 4 jets, $t\bar{t}$ production can also contribute to the $\ell\nu + 1$ jet channel if only one b-tag is required. Top pair events where the b-quark in $t \to b\ell\nu$ is not detected, and the two light quark jets in $t \to bjj$ are either missed or are merged with the tagged b-quark are the dominant source for signal $\ell\nu b$ events. The Wb invariant mass distribution thus may still carry useful information on heavy $t\bar{t}$ resonances. However, as shown in Fig. 12, the background from $W + 1$ jet production where the jet is misidentified as a b-quark is much larger than the signal. Since the b-jet from $t \to b\ell\nu$ is usually lost, a m_T cut is ineffective. Furthermore, it prevents reconstruction of the top quark transverse momentum. A cut on the jet invariant mass may help to reduce the background (see Sec. IV). However, any gain in the signal to background ratio from such a cut is at least partially canceled by a reduced b-tagging efficiency and an enhanced light jet mistagging probability at large invariant masses. Furthermore, the $\ell\nu + 1$ jet cross section is sig-

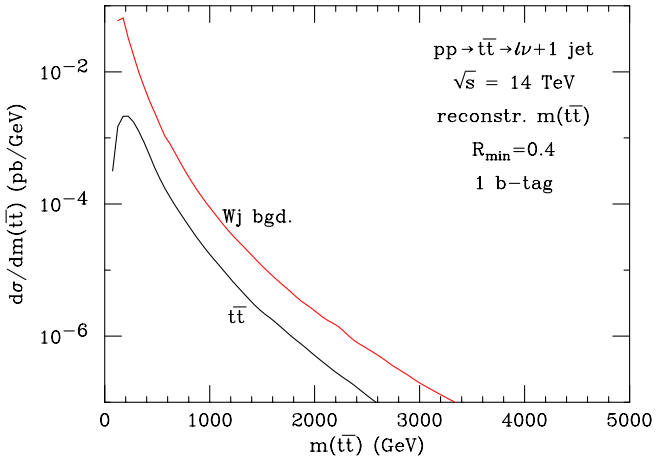

FIG. 12 (color online). The LO differential cross section of the SM $t\bar{t} \to \ell\nu + 1$ jet signal (black) and the Wj background (red) as a function of the reconstructed $t\bar{t}$ (Wb) invariant mass at the LHC. The jet is assumed to be b-tagged. The cuts imposed are listed in Eqs. (4)–(7). In addition an isolation cut [see Eq. (8)] with $R_{\min} = 0.4$ is imposed.

nificantly smaller than that in the 2, 3, and 4 jet channels (see below) at large values of the reconstructed $t\bar{t}$ invariant mass. We will not consider the $\ell\nu + 1$ jet final state further here.

The $m(t\bar{t})$ and $p_T(t \to b\ell\nu)$ distributions of the signal and the combined background in the $\ell\nu + 2$ jets final state with one b-tag are shown in Fig. 13. Even when a m_T cut is imposed in addition to the standard transverse momentum, rapidity and separation cuts, the background is still considerably larger than the signal in the $t\bar{t}$ invariant mass distribution. In the $p_T(t)$ distribution, the signal to background ratio is more favorable. Requiring $|m_T - m_t| < 20$ GeV, signal and background are approximately equal at large p_T.

In final states with two b-tags we used the b-jet with the smaller separation from the charged lepton to reconstruct

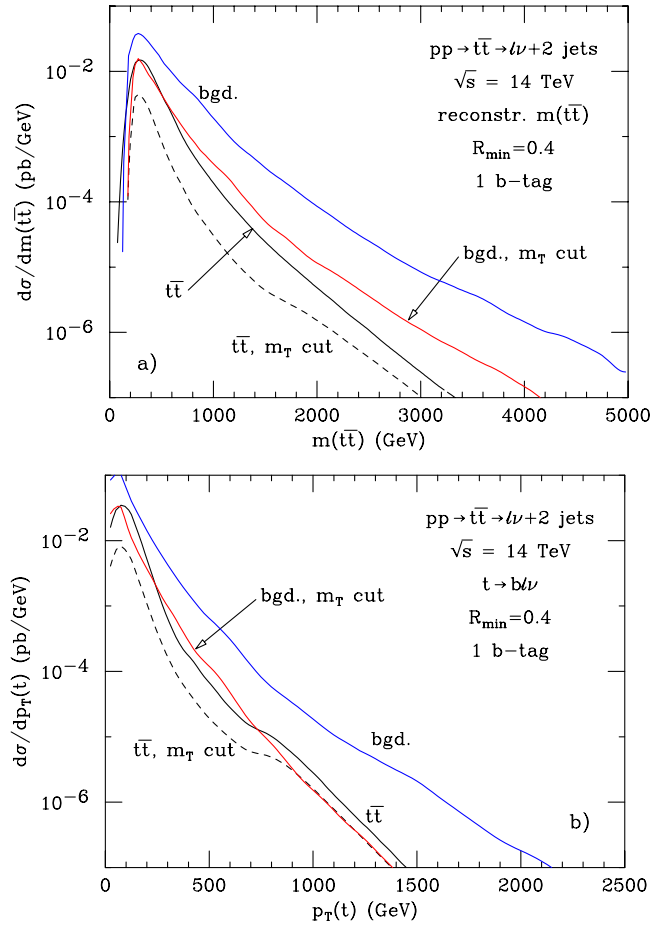

FIG. 13 (color online). The LO differential cross section of the SM $t\bar{t} \to \ell\nu + 2$ jets signal and the combined background as a function of (a) the reconstructed $t\bar{t}$ invariant mass and (b) the $t \to b\ell\nu$ transverse momentum at the LHC. One of the jets is assumed to be b-tagged. The black and blue curves show the signal and background, respectively, imposing standard cuts [Eqs. (4)–(8)] with $R_{\min} = 0.4$. The dashed and red curves show signal and background if in addition a cluster transverse mass cut is imposed on the $b\ell\nu$ system [see Eq. (17)].

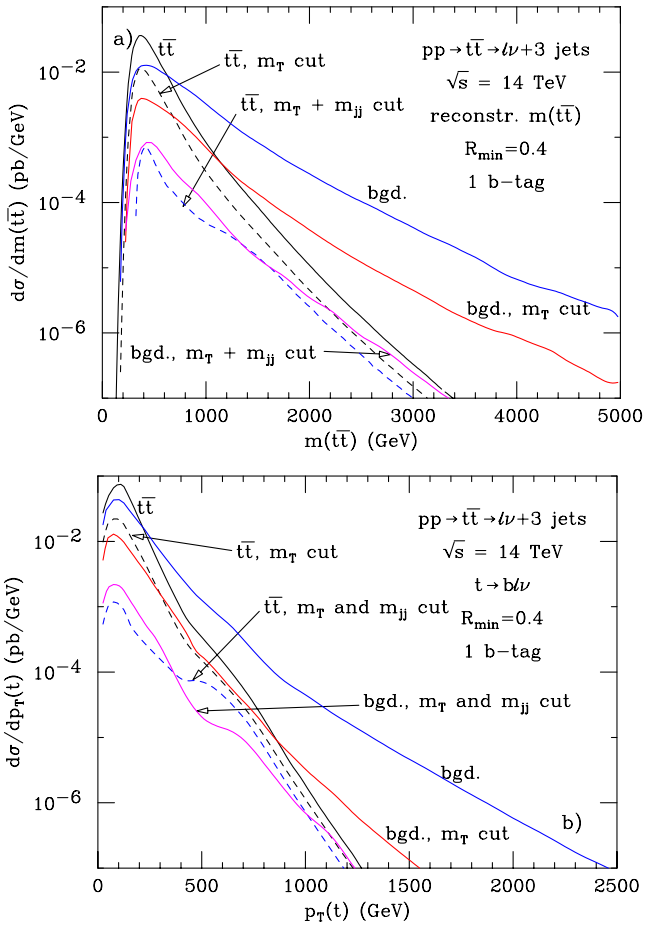

FIG. 14 (color online). The LO differential cross section of the SM $t\bar{t} \to \ell\nu + 3$ jets signal and the combined background as a function of (a) the reconstructed $t\bar{t}$ invariant mass and (b) the $t \to b\ell\nu$ transverse momentum at the LHC. One of the jets is assumed to be b-tagged. The black and blue curves show the signal and background, respectively, imposing standard cuts [Eqs. (4)–(8)] with $R_{\min} = 0.4$. The dashed and red curves show signal and background if in addition a cluster transverse mass cut is imposed on the $b\ell\nu$ system [see Eq. (17)]. The blue dashed and magenta curves, finally, show signal and background if in addition the invariant mass cut of Eq. (18) is imposed.

$p_T(t \to b\ell\nu)$ and to compute m_T. Now, with only one b-tag, we use the jet, $j_{\min}$, whether it is tagged or not, which is closest to the charged lepton in ΔR, i.e. we require

$$|m_T(j_{\min}\ell) - m_t| < 20 \text{ GeV}. \tag{17}$$

If only the standard cuts of Eqs. (4)–(8) are imposed, Wjj production is the dominant background source for the $\ell\nu + 2$ jet final state with one b-tag. If we require in addition that the $j_{\min}\ell\nu$ cluster transverse mass satisfies Eq. (17), $pp \to Wjj$ and $pp \to tj$ each contribute about one-half of the total background.

To improve the signal to background ratio, one may consider a cut on the invariant mass of the jet with the

larger separation from the charged lepton. This will be discussed in more detail in Sec. IV.

In Fig. 14 we show signal and background predictions for the 3 jet final state. Even when we require

$$|m(j_2 j_3) - m_t| < 20 \text{ GeV} \tag{18}$$

in addition to the m_T cut, the background is found to be somewhat larger than the signal in the $m(t\bar{t})$ distribution. j_2 and j_3 in Eq. (18) are the jets with the larger separations from the charged lepton. The signal to background ratio is slightly better in the $p_T(t)$ distribution. Without the $m(j_2 j_3)$ cut, the background is dominated by $W + 3$ jet production. If the invariant mass cut of Eq. (18) is imposed, $W + 3$ jet, Wjt, and Wbt production all contribute about equally to the background.

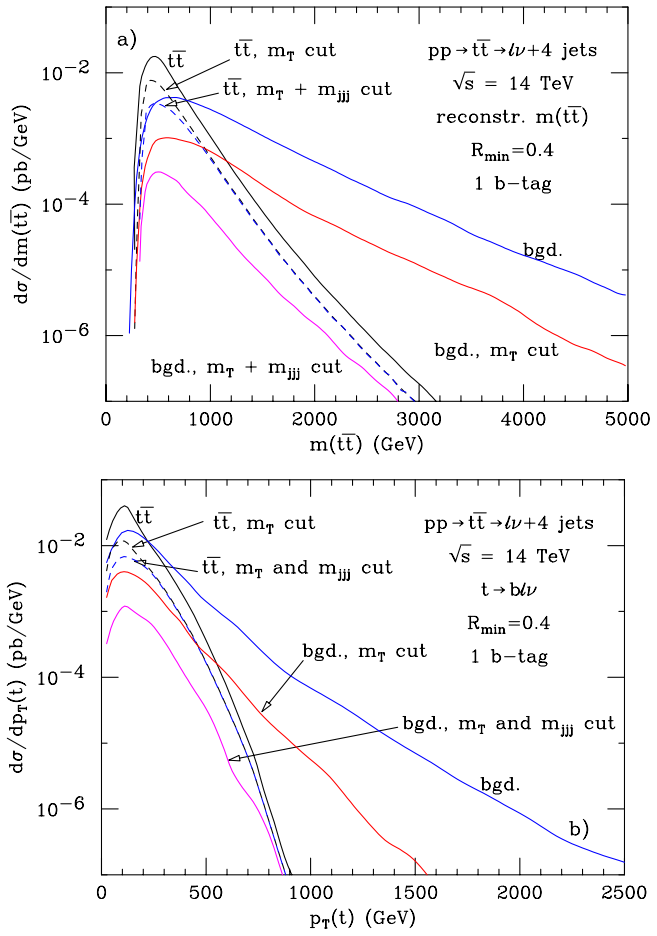

FIG. 15 (color online). The LO differential cross section of the SM $t\bar{t} \to \ell\nu + 4$ jets signal and the combined background as a function of (a) the reconstructed $t\bar{t}$ invariant mass and (b) the $t \to b\ell\nu$ transverse momentum at the LHC. One of the jets is assumed to be b-tagged. The black and blue curves show the signal and background, respectively, imposing standard cuts [Eqs. (4)–(8)] with $R_{\text{min}} = 0.4$. The dashed and red curves show signal and background if in addition a cluster transverse mass cut is imposed on the $b\ell\nu$ system [see Eq. (17)]. The blue dashed and magenta curves, finally, show signal and background if in addition the invariant mass cut of Eq. (19) is imposed.

In Fig. 15, finally, we show signal and background for the 4 jet final state. Once a m_T and an

$$|m(j_2 j_3 j_4) - m_t| < 20 \text{ GeV} \tag{19}$$

invariant mass cut have been imposed, the background is considerably smaller than the signal. j_2, j_3, and j_4 in Eq. (19) are the three jets with the larger separations from the charged lepton. Without the $m(j_2 j_3 j_4)$ cut, the background is dominated by $W + 4$ jet production. If Eq. (19) is imposed, $W + 4$ jet, Wjt, and Wbt production all contribute about equally to the background.

For $\epsilon_b = 0.2$ and $P_{j\to b} = 1/30$, as suggested in Refs. [6,19], the signal to background ratio in the TeV region would be about a factor 2 (factor 5) worse than the results shown in Figs. 13–15 (Fig. 12).

IV. A JET INVARIANT MASS CUT

In Sec. III we have seen that a cut on the $j\ell\nu$ cluster transverse mass is not sufficient to suppress the background to an acceptable level in the $\ell\nu + 2$ jets final state with one b-tag. At large $t\bar{t}$ invariant mass, events where the jets from $t \to bjj$ all merge into a single t-jet dominate the signal. The invariant mass of such a t-jet is consistent with the top quark mass. The t-jet usually is the jet with the larger separation from the charged lepton. The main background for the $\ell\nu + 2$ jets final state with one b-tag originates from Wjj and $(t + \bar{t})j$, $t \to b\ell\nu$, (t-channel single top) production. In both processes, the jet which is further away from the charged lepton in $\eta - \phi$ space is a light quark or gluon jet. At LO, such jets are (almost) massless. Once higher order QCD corrections are taken into account, light quark or gluon jets acquire a mass which depends on the jet algorithm and the distance in ΔR space used to cluster particles. The average invariant mass of such a jet is expected to be [55]

$$\langle m(j) \rangle \propto \sqrt{\alpha_s} p_T(j). \tag{20}$$

This suggests that a cut on the invariant mass of the jet with the larger separation from the charged lepton may be helpful in suppressing the background in the $\ell\nu + 2$ jets final state with one b-tag. As discussed in Sec. II B, such a cut would also be helpful in reducing the combinatorial background from extra QCD jets.

For both Wjj and $(t + \bar{t})j$ production, the NLO QCD corrections are known [47,50]. However, nonperturbative QCD effects may significantly contribute to the invariant mass of a light quark or gluon jet. Calculations which only include NLO QCD corrections may therefore not be reliable in predicting how well a jet invariant mass cut reduces the background in the $\ell\nu + 2$ jets final state with one b-tag.

In order to *estimate* the effect of a jet invariant mass cut on the Wjj and $(t + \bar{t})j$ background, we convolute the

differential cross sections obtained from ALPGEN and MADEVENT with $\mathcal{P}(m(j_{\rm top}), p_T(j_{\rm top}))$, where $j_{\rm top}$ is the jet with the larger separation from the charged lepton (i.e. the t-jet candidate). A cut on $m(j_{\rm top})$ is then imposed (see below). $\mathcal{P}(m(j), p_T(j))$ is the two-dimensional probability density that a jet with transverse momentum $p_T(j)$ has an invariant mass $m(j)$. We calculate $\mathcal{P}(m(j), p_T(j))$ by generating 10^5 W + jets events in PYTHIA [56] and passing them through PGS4 [57], which simulates the response of a generic high-energy physics collider detector with a tracking system, electromagnetic and hadronic calorimetry, and muon system. Jets are required to have $p_T(j) > 30$ GeV. The rapidity coverage of the tracking system is assumed to be $|\eta| < 3$. Jets are reconstructed in the cone [58] and k_T algorithms [59] as implemented in PGS4, using a cone size (D parameter) of $R = 0.5$ ($D = 0.5$) in the cone (k_T) algorithm. Since it is infrared safe, the k_T algorithm is the theoretically preferred algorithm. For a discussion of the advantages and disadvantages of the two algorithms at hadron colliders, see Ref. [60]. The cone size (D parameter) is deliberately chosen to be slightly larger than in our parton level studies to avoid drawing conclusions which are too optimistic.

We find that the probability density function, $\mathcal{P}$, for the k_T algorithm has a much longer tail at large jet invariant masses than for the cone algorithm. This is illustrated in Fig. 16, where we show the one-dimensional probability density $P(x)$, $x = m(j)/p_T(j)$, for W + jets events with $p_T(j) > 30$ GeV. Very similar results are obtained for jets in other processes, such as t-channel single top production. $P(x)$ peaks at $x \approx 0.1$–0.13 for both algorithms. In the cone algorithm, a jet has a fixed size in $\eta - \phi$ space.

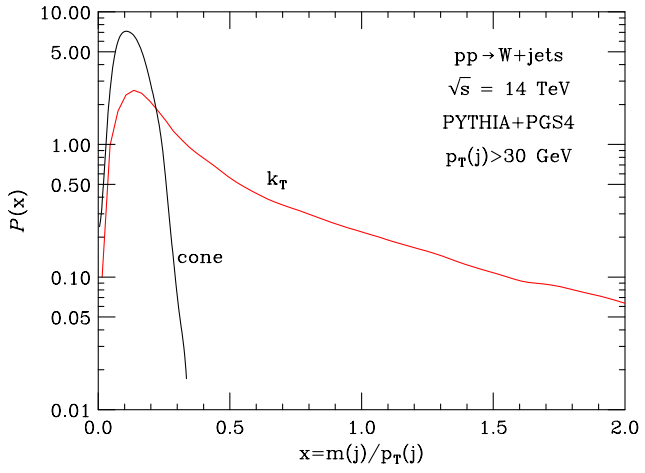

FIG. 16 (color online). The probability density $P(x)$ versus $x = m(j)/p_T(j)$ for a jet with transverse momentum $p_T(j)$ to have an invariant mass $m(j)$ in $pp \to W$ + jets at the LHC. Shown are results for the cone (black) and the k_T jet algorithm (red). The W + jets events are generated with PYTHIA requiring $p_T(j) > 30$ GeV and then processed into physics objects using PGS4. The PGS4 parameters used are described in the text.

This limits the jet invariant mass. For the parameters chosen here, it is very difficult for a jet in the cone algorithm to have an invariant mass larger than about $0.3 \cdot p_T(j)$. In contrast, the k_T algorithm has a tendency to "vacuum up" contributions from the underlying event, and k_T jets therefore do not have a well-defined size. As a result, the k_T jet mass tail extends to $x = 1$ and beyond and is sensitive to how the underlying event is simulated.

Figure 16 shows $P(x)$ for jets with $p_T(j) > 30$ GeV. For a higher p_T threshold, the x value for which the distribution peaks remains almost constant. However, $P(x)$ falls considerably faster with x for larger $p_T(j)$ values when using the k_T algorithm. Removing the contributions from the underlying event, or decreasing the D parameter, leads to a similar result.

The differences between $\mathcal{P}(m(j), p_T(j))$ in the k_T and the cone algorithm have a significant impact on the background in the $m(t\bar{t})$ distribution of the $\ell\nu + 2$ jet final state with one b-tag when a

$$|m(j_{\rm top}) - m_t| < 20 \text{ GeV} \tag{21}$$

cut is imposed. This is shown in Fig. 17(a), where, in addition to the jet invariant mass cut, we also impose the cluster transverse mass cut of Eq. (17). $j_{\rm top}$ in the figure denotes the t-jet resulting from $t \to bjj$. The key in understanding the significant dependence of the background on the jet algorithm in the $m(t\bar{t})$ distribution is the observation that a large fraction of the $\ell\nu + 2$ jet background events at high invariant mass contains a jet with a relatively small p_T. If the cone algorithm is used, a jet transverse momentum of at least 450 GeV is needed to satisfy Eq. (21). This is not the case for the k_T algorithm, where jets with a p_T as low as 75 GeV may pass the jet invariant mass cut. In the cone algorithm, the Wjj and tj backgrounds, which dominate if no $m(j_{\rm top})$ cut is imposed, thus are negligible compared with the Wbt and Wjt, $t \to bjj$, background. On the other hand, if the k_T algorithm is used, $pp \to Wjj$ and $pp \to tj$ are still the dominant background sources. Note that the $m(j_{\rm top})$ invariant mass cut [Eq. (21)] has no effect on the Wbt and Wjt background.

In either case, the jet invariant mass cut strongly suppresses the background. It also decimates the signal for $m(t\bar{t}) < 1.6$ TeV, eliminating all events where one or two jets are not passing the acceptance cuts of Eq. (5). For larger $t\bar{t}$ invariant masses, the $m(j_{\rm top})$ cut reduces the signal by at most a factor 2. In this region the signal to background ratio is $\mathcal{O}(1)$ or better, an improvement of a factor 10 or more compared with the result without such a cut [see Fig. 13(a)]. If one were able to eliminate the effect of the underlying event on the jet invariant mass in the k_T algorithm, the background could be reduced by an additional factor 2.

Since the Wjj and tj contributions to the background at large $p_T(t)$ are smaller than at large $m(t\bar{t})$ once the jet invariant mass cut has been imposed, the background

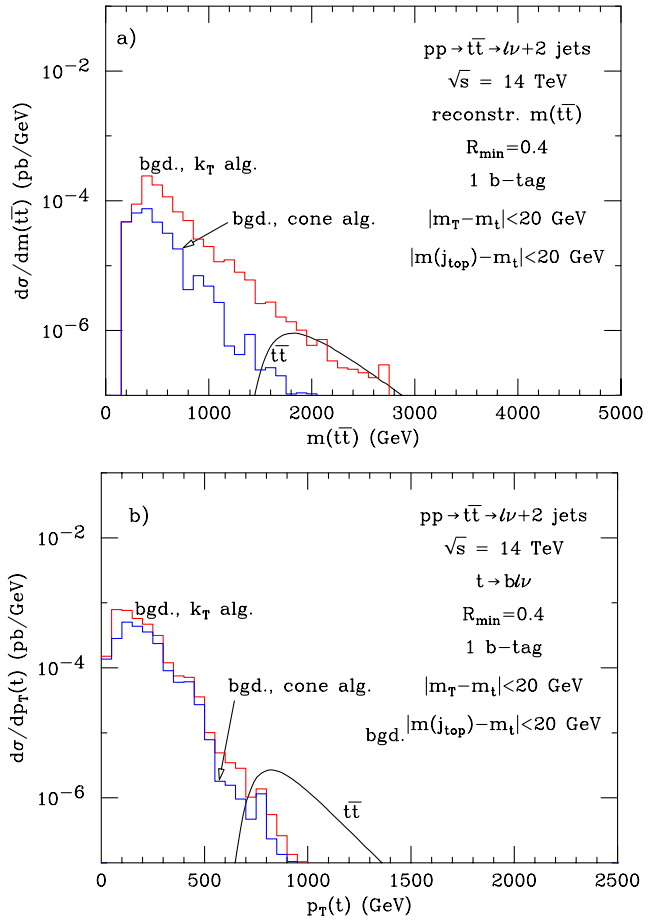

FIG. 17 (color online). The LO differential cross section of the SM $t\bar{t} \to \ell\nu + 2$ jets signal and the combined background as a function of (a) the reconstructed $t\bar{t}$ invariant mass and (b) the $t \to b\ell\nu$ transverse momentum at the LHC. One of the jets is assumed to be b-tagged. In addition to the standard cuts [Eqs. (4)–(8)] with $R_{\rm min} = 0.4$ a $|m_T - m_t| < 20$ GeV [see Eq. (17)] and a $|m(j_{\rm top}) - m_t| < 20$ GeV cut are imposed. The black curve shows the $t\bar{t}$ signal cross section. The red and blue histograms are the predictions for the combined background using the k_T and cone algorithms, respectively. As before, we assume $\epsilon_b = 0.6$ and $P_{j\to b} = 1/100$.

$p_T(t)$ distribution, which is shown in Fig. 17(b), is found to be much less sensitive to the details of the jet algorithm. For $p_T(t) > 700$ GeV, the $t\bar{t}$ signal dominates over the background. Wjt production is the largest background source in the $p_T(j)$ distribution in the 2 jet final state with one b-tag when a cluster transverse mass cut and a jet invariant mass cut are imposed. Comparing the results of Fig. 17(b) with those of Figs. 14(b) and 15(b) shows that, once an invariant mass cut on the jet(s) originating from the hadronic top decay has been imposed, the 2 jet final state is by far the largest source for $t\bar{t}$ events with $p_T(t) >$ 900 GeV. Furthermore, the signal to background ratio in the 2 jet channel in this region is considerably better than that for the 3 jet and 4 jet final states.

As before, we have used $\epsilon_b = 0.6$ and $R_{j\to b} = 1/100$ in the numerical results presented in this section. If the b-tagging efficiency is reduced by a factor 3 in the TeV region, and $R_{j\to b}$ simultaneously increases by a factor 3, the signal to background ratio worsens by about a factor 1.5–3.

From the calculations presented in this section, we conclude that a jet invariant mass cut may be useful in improving the signal to background ratio in the $\ell\nu + 2$ jet final state with one b-tag. Details, however, may depend on the jet algorithm used. Our calculation uses a rather crude approximation to model the invariant mass of a light quark or gluon jet. Our results thus should be viewed as order of magnitude estimates. The main disadvantage of the jet invariant mass cut clearly is that only few signal events will survive it.

V. SUMMARY AND CONCLUSIONS

Many new physics models predict the existence of $t\bar{t}$ resonances with masses in the TeV region. New particles with mass M which decay into a $t\bar{t}$ pair lead to a peak in the $t\bar{t}$ invariant mass distribution located at $m(t\bar{t}) = M$ and to a Jacobian peak at $p_T(t) = M/2$ in the top quark transverse momentum distribution. The lepton + jets final state offers a good opportunity to search for such particles. The dilepton channel suffers from a small branching ratio and the inability to reconstruct the $t\bar{t}$ invariant mass and the top quark transverse momentum. The all-hadronic final state is subject to a very large QCD background which limits the sensitivity to new physics.

The search for resonances in the $t\bar{t}$ channel with masses in the TeV region requires the reconstruction of very energetic top quarks. These are strongly boosted, and their decay products are highly collimated. This leads to overlapping and merging jets from hadronically decaying top quarks. As a result, the standard $t\bar{t}$ identification requirements for the lepton + jets final state—an isolated charged lepton, missing transverse momentum and four isolated jets with two b-tags—strongly reduce the observable $t\bar{t}$ cross section. In addition, the tagging efficiency for b-quarks in $t\bar{t}$ events with very energetic top quarks may be up to a factor 3 smaller than at low energies. This further reduces the number of $t\bar{t}$ events which can be identified using standard $t\bar{t}$ identification requirements.

In this paper we investigated in detail how the efficiency for detecting very energetic top quarks in the lepton + jets channel can be improved. We found that the $\ell\nu + n$ jets ($\ell = e, \mu$) final states with $n = 2$ and $n = 3$, and one or two b-tags, increase the observable rate significantly. For s-channel resonances, the gain is even larger. In particular, $\ell\nu + n$ jets events with only one b-tag offer a crucial advantage in the TeV region, provided that the background can be controlled.

Using MC@NLO, we investigated how NLO QCD corrections affect the lepton + jets final states at very high

energies. We found that QCD corrections in this channel are large, often produce extra hard jets from radiation in the $t\bar{t}$ production process, and may substantially modify the p_T distribution of top quarks in the high transverse momentum region. Details depend on how many jets from the hadronic top decay are observed. When final state topologies with a fixed number of jets are considered and invariant mass cuts on the observed $t \to bjj$ jets are imposed, the radiation of extra quarks and gluons is strongly reduced, and QCD corrections are moderate and decrease with increasing $m(t\bar{t})$ and $p_T(t)$. In the TeV region, the ratio of NLO to LO differential cross sections typically is 0.7–0.8 if one requires $p_T(t\bar{t}) < 100$ GeV.

We also presented a comprehensive analysis of the background processes which contribute to the $\ell\nu + n$ jets final states with one or two b-tags. All relevant $W +$ jets and single top background processes were considered. In the 2 jet and 3 jet final states, the background processes occur at a lower order in perturbation theory, and thus are potentially more worrisome, than in the 4 jet channel, in particular, if only one b-quark is tagged. We found that a cluster transverse mass cut on the $t \to b\ell\nu$ system is sufficient to adequately suppress the background in the $\ell\nu + 2$ jet channel with two b-tags. In the 3 jet and 4 jet final states with two tagged b-jets, an additional cut on the invariant mass of the observed $t \to bjj$ jets is needed in order to achieve a signal to background ratio better than one over the entire kinematic region of interest.

As expected, the background is significantly higher if only one b-quark is tagged. In the 2 jet channel, an invariant mass cut on the t-jet which results from $t \to bjj$ is needed to suppress the background sufficiently. We simulated the effect of such a cut on the background by convoluting the two-dimensional probability density that a light quark or gluon jet with a given p_T has a jet mass $m(j)$ with the differential cross section of the relevant background processes. The probability density was determined for both the k_T and the cone algorithm using PYTHIA and PGS4. For the $t\bar{t}$ invariant mass distribution we found that the background differential cross section significantly depends on the jet algorithm used. For the 3 jet final state, the background in the $m(t\bar{t})$ distribution is somewhat larger than the signal even after imposing a cluster transverse mass cut and a cut on the invariant mass of the jets originating from $t \to bjj$ [see Fig. 14(a)]. The signal to background ratio in the $p_T(t)$ distribution in all cases is better than in the $t\bar{t}$ invariant mass distribution. Although we presented all numerical results for a b-tagging efficiency of $\epsilon_b = 60\%$ and a light jet mistagging probability of $P_{j\to b} = 1\%$ which are only valid in the sub-TeV region, we commented on how our results change if ϵ_b decreases, and $P_{j\to b}$ simultaneously increases, by a factor 3 in the TeV region, as indicated by ATLAS simulations [6,19].

From the numerical results presented in Secs. III and IV, it thus may not be clear how good or bad the signal to background ratio is, and whether a $t\bar{t}$ resonance with a mass in the TeV region can be observed, for the worst-case scenario of $\epsilon_b = 0.2$, $P_{j\to b} = 1/30$, if one or two jets are b-tagged, and the 2 jet, 3 jet, and 4 jet final states are combined. To answer this question, we show the LO $m(t\bar{t})$ and $p_T(t)$ distributions for these parameters in Fig. 18. As before, we have imposed the standard acceptance cuts of Eqs. (4)–(8)) with $R_{\rm min} = 0.4$. In addition, events are assumed to satisfy the cluster transverse mass cuts, Eqs. (13) and (17), and the invariant mass cuts of Eqs. (15), (16), (18), and (19). In order to be conservative, we have used the background obtained with the k_T algorithm for the contribution from the 2 jet final state with one

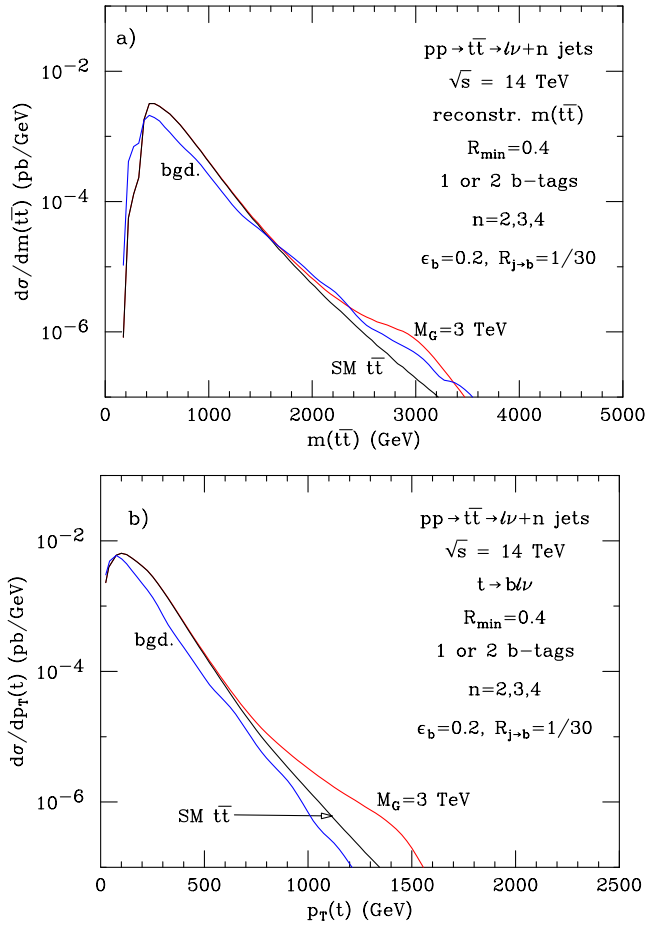

FIG. 18 (color online). The LO differential cross section of the combined SM $t\bar{t} \to \ell\nu + n$ jets ($n = 2, 3, 4$) signal (black line), a bulk RS KK gluon, G, with $M_G = 3$ TeV (red line), and the combined background (blue line) as a function of (a) the reconstructed $t\bar{t}$ invariant mass and (b) the $t \to b\ell\nu$ transverse momentum at the LHC. One or two of the jets are assumed to be b-tagged. In addition to the standard cuts [Eqs. (4)–(8)] with $R_{\rm min} = 0.4$ a $|m_T - m_t| < 20$ GeV cut, and a cut on the invariant mass, m, of the jet(s) from $t \to bjj$ of $|m - m_t| < 20$ GeV are imposed in all cases except for $n = 2$ and two tagged b-jets where the m-cut has not been imposed. We assume $\epsilon_b = 0.2$ and $P_{j\to b} = 1/30$.

b-tag. We emphasize that, for $t\bar{t}$ invariant masses below about 2 TeV, and top quark transverse momenta smaller than 600 GeV, our results are probably overly pessimistic as the b-tagging efficiency in this region should be significantly higher, and the light jet mistagging probability considerably lower, than what we have assumed in Fig. 18.

The black lines in Fig. 18 represent the SM $t\bar{t}$ signal. The red lines show the prediction for a bulk RS KK gluon with mass $M_G = 3$ TeV. The blue curves, finally, represent the combined background. For an integrated luminosity of 100 fb^{-1}, a $M_G = 3$ TeV bulk RS KK gluon leads to about 100 (130) signal events for $m(t\bar{t}) \geq 2$ TeV [$p_T(t) \geq 700$ GeV] on a total background [SM $t\bar{t}$ production (red lines) and other backgrounds (blue lines) combined] of about 400 (350) events. This corresponds to about a 5σ signal in the invariant mass distribution, and to about a 7σ effect in the $p_T(t)$ differential cross section, reflecting the smaller background in the top quark transverse momentum distribution. For comparison, if one were to consider the 4 jet final state with two b-tags only, less than one signal event would be expected.

The significances given here are for illustration purposes only. All calculations have been performed at LO, and thus retain a significant dependence on the factorization and renormalization scales. This could easily change the signal to background ratio by a factor 2. Nevertheless, it is clear that lepton + jets topologies with less than 4 jets and/or only one b-tag will be able to significantly enhance the capabilities of the LHC experiments in discovering resonances in the $t\bar{t}$ channel, even if the b-tagging efficiency and the light jet mistagging probability in the TeV region are much worse than at low energies.

Figure 18 also demonstrates that the cluster transverse mass and invariant mass cuts imposed using the techniques described in Sec. III work well in suppressing the W + jets and single top background at large energies. As noted before, these cuts also suppress the radiation of extra QCD jets especially at high energies. For example, in an event where all $t \to bjj$ jets merge into a single jet and where there are one or two extra QCD jets, the invariant mass of the two or three jets in the final state will usually not be in the vicinity of m_t. However, for a more quantitative statement on how well a $t \to bjj$ jet(s) invariant mass cut suppresses extra QCD radiation, detailed simulations are needed which are beyond the scope of this paper.

While the non-$t\bar{t}$ background in the invariant mass distribution does not seriously impact the search for a strongly coupled resonance in the $t\bar{t}$ channel such as a bulk RS KK gluon, it will considerably limit the search for weakly coupled resonances. In order to further reduce the background, one can try to make use of the substructure of jets in $t\bar{t}$ events in the 2 jet and 3 jet final states. In the 2 jet final state, the single t-jet from $t \to bjj$ contains two light quark jets which form a W boson. In the 3 jet channel, the b-jet receives contributions from merging with one of the light quark jets, while the second (nontaggable) jet has a component originating from the merging of the two jets from W decay. The invariant mass distribution of these jets thus should differ from that of QCD jets. Other possibilities to discriminate $t\bar{t}$ and background events include track isolation [61], and identifying the substructure of jets using methods such as those proposed in Refs. [37,38].

We also reemphasize the importance of more accurate estimates of the b-tagging efficiency ϵ_b for top events at very high energies. Existing calculations [6,19] indicate that ϵ_b may be significantly smaller in this region than at low energies. Overlapping and merging jets in lepton + jets events with 2 or 3 jets are likely to further complicate the reconstruction of secondary vertices.

ACKNOWLEDGMENTS

We would like to thank B. Acharya, A. Belyaev, M. A. Dufour, B. Knuteson, T. LeCompte, B. Lillie, S. Mrenna, and B. Vachon for useful discussions. We are also grateful to J. Huston for a private tutorial on jet algorithms. One of us would like to thank the Fermilab Theory Group and the High Energy Physics Group, McGill University, where part of this work was done, for their generous hospitality. This research was supported in part by the National Science Foundation under Grant No. PHY-0456681 and the Department of Energy under Grant No. DE-FG02-91ER40685.

APPENDIX: MOMENTUM SMEARING AND b-JET ENERGY LOSS

We simulate detector response by Gaussian smearing of the four momenta of quarks, gluons, and charged leptons according to ATLAS expectations [27]:

$$\frac{\Delta E}{E}(\text{had}) = \frac{0.5}{\sqrt{E}} \oplus 0.03 \qquad (|\eta| < 3.0)$$

$$\frac{\Delta E}{E}(\text{lep}) = \frac{0.095}{\sqrt{E}} \oplus 0.005 \qquad (|\eta| < 2.5).$$

Here, η is the pseudorapidity, E is the energy measured in GeV, and the $\oplus$ sign symbolizes that the two terms are added in quadrature. For simplicity we smear electron and muon momenta using the same resolution.

The energy loss of b-jets is due to the neutrino produced in semileptonic b-decays and $b \to c$ decays with subsequent semileptonic charm decay. It is simulated by scaling down the b-quark three momentum vector, $\vec{p}$, by a random factor z which is determined from a fit to the energy spectrum of the neutrino. The following values of z are used:

$$
\begin{aligned}
z &= 1 \quad && \text{for } 0 < x < 0.6 \\
z &= 0.95 \quad && \text{for } 0.6 \le x < 0.75 \\
z &= 0.85 \quad && \text{for } 0.75 \le x < 0.854 \\
z &= 0.75 \quad && \text{for } 0.854 \le x < 0.923 \\
z &= 0.65 \quad && \text{for } 0.923 \le x < 0.964 \\
z &= 0.55 \quad && \text{for } 0.964 \le x < 0.987 \\
z &= 0.45 \quad && \text{for } 0.987 \le x < 0.9965 \\
z &= 0.35 \quad && \text{for } 0.9965 \le x < 0.9995 \\
z &= 0.25 \quad && \text{for } 0.9965 \le x < 1,
\end{aligned}
$$

where $0 < x < 1$ is a pseudorandom number. The rescaled b-quark energy is given by $E_r^2(b) = m_b^2 + z^2\vec{p}^2$, where $m_b = 4.8$ GeV is the b-quark mass.

[1] M. Beneke *et al.*, arXiv:hep-ph/0003033.
[2] C. T. Hill, Phys. Lett. B **266**, 419 (1991); **345**, 483 (1995); C. T. Hill and S. J. Parke, Phys. Rev. D **49**, 4454 (1994); R. M. Harris, C. T. Hill and S. J. Parke, arXiv:hep-ph/9911288; B. A. Dobrescu and C. T. Hill, Phys. Rev. Lett. **81**, 2634 (1998); R. S. Chivukula, B. A. Dobrescu, H. Georgi, and C. T. Hill, Phys. Rev. D **59**, 075003 (1999).
[3] For a review, see C. T. Hill and E. H. Simmons, Phys. Rep. **381**, 235 (2003); **390**, 553(E) (2004).
[4] N. Arkani-Hamed, A. G. Cohen, and H. Georgi, Phys. Lett. B **513**, 232 (2001); N. Arkani-Hamed, A. G. Cohen, T. Gregoire, and J. G. Wacker, J. High Energy Phys. 08 (2002) 020; N. Arkani-Hamed, A. G. Cohen, E. Katz, A. E. Nelson, T. Gregoire, and J. G. Wacker, J. High Energy Phys. 08 (2002) 021; N. Arkani-Hamed, A. G. Cohen, E. Katz, and A. E. Nelson, J. High Energy Phys. 07 (2002) 034; I. Low, W. Skiba, and D. Smith, Phys. Rev. D **66**, 072001 (2002); T. Han, H. E. Logan, B. McElrath, and L. T. Wang, Phys. Rev. D **67**, 095004 (2003); G. Azuelos *et al.*, Eur. Phys. J. C **39S2**, 13 (2005).
[5] For a review, see M. Schmaltz and D. Tucker-Smith, Annu. Rev. Nucl. Part. Sci. **55**, 229 (2005).
[6] S. González de la Hoz, L. March, and E. Ros, Report No. ATL-PHYS-PUB-2006-003.
[7] N. Arkani-Hamed, S. Dimopoulos, and G. R. Dvali, Phys. Lett. B **429**, 263 (1998).
[8] L. Randall and R. Sundrum, Phys. Rev. Lett. **83**, 3370 (1999).
[9] I. Antoniadis, Phys. Lett. B **246**, 377 (1990); J. D. Lykken, Phys. Rev. D **54**, R3693 (1996); I. Antoniadis and M. Quiros, Phys. Lett. B **392**, 61 (1997).
[10] A. L. Fitzpatrick, J. Kaplan, L. Randall, and L. T. Wang, J. High Energy Phys. 09 (2007) 013.
[11] M. Arai, N. Okada, K. Smolek, and V. Simak, Phys. Rev. D **70**, 115015 (2004); **75**, 095008 (2007).
[12] C. D. McMullen and S. Nandi, arXiv:hep-ph/0110275.
[13] K. Agashe, A. Delgado, M. J. May, and R. Sundrum, J. High Energy Phys. 08 (2003) 050; K. Agashe, A. Belyaev, T. Krupovnickas, G. Perez, and J. Virzi, arXiv:hep-ph/0612015.
[14] B. Lillie, L. Randall, and L. T. Wang, J. High Energy Phys. 09 (2007) 074.
[15] B. Lillie, J. Shu, and T. Tait, arXiv:0706.3960.
[16] A. Djouadi, G. Moreau, and R. K. Singh, arXiv:0706.4191.
[17] R. Ghavri, C. D. McMullen, and S. Nandi, Phys. Rev. D **74**, 015012 (2006).
[18] D. A. Dicus, C. D. McMullen, and S. Nandi, Phys. Rev. D **65**, 076007 (2002).
[19] L. March, E. Ros, and B. Salvachúa, Report No. ATLAS-PHYS-PUB-2006-002.
[20] G. Burdman, B. A. Dobrescu, and E. Ponton, Phys. Rev. D **74**, 075008 (2006).
[21] A. S. Belyaev, I. L. Shapiro, and M. A. B. do Vale, Phys. Rev. D **75**, 034014 (2007).
[22] E. Eichten and K. D. Lane, Phys. Lett. B **327**, 129 (1994); **352**, 382 (1995).
[23] E. Cogneras and D. Pallin, ATL-PHYS-PUB-2006-033.
[24] P. H. Frampton and S. L. Glashow, Phys. Lett. B **190**, 157 (1987); Phys. Rev. Lett. **58**, 2168 (1987); M. A. Doncheski and R. W. Robinett, Phys. Lett. B **412**, 91 (1997).
[25] E. H. Simmons, Phys. Rev. D **55**, 1678 (1997).
[26] D. Choudhury, R. M. Godbole, R. K. Singh, and K. Wagh, arXiv:0705.1499.
[27] A. Airapetian *et al.* (ATLAS Collaboration), Report No. CERN/LHCC/99-15.
[28] G. L. Bayatian *et al.* (CMS Collaboration), Report No. CERN/LHCC 2006/021.
[29] F. Abe *et al.* (CDF Collaboration), Phys. Rev. Lett. **74**, 2626 (1995).
[30] S. Abachi *et al.* (D0 Collaboration), Phys. Rev. Lett. **74**, 2632 (1995).
[31] J. Pumplin, D. R. Stump, J. Huston, H. L. Lai, P. Nadolsky, and W. K. Tung, J. High Energy Phys. 07 (2002) 012.
[32] CDF and D0 Collaborations, arXiv:hep-ex/0703034.
[33] M. L. Mangano, M. Moretti, F. Piccinini, R. Pittau, and A. D. Polosa, J. High Energy Phys. 07 (2003) 001.
[34] V. Barger, T. Han, and D. G. E. Walker, arXiv:hep-ph/0612016.
[35] A. A. Affolder *et al.* (CDF Collaboration), Phys. Rev. Lett. **87**, 102001 (2001).

[36] B. Vachon (private communication).
[37] J. M. Butterworth, J. R. Ellis and A. R. Raklev, J. High Energy Phys. 05 (2007) 033.
[38] J. M. Butterworth, B. E. Cox, and J. R. Forshaw, Phys. Rev. D **65**, 096014 (2002).
[39] P. Nason, S. Dawson, and R. K. Ellis, Nucl. Phys. **B303**, 607 (1988); **B327**, 49 (1989); **B335**, 260(E) (1990); W. Beenakker, H. Kuijf, W. L. van Neerven, and J. Smith, Phys. Rev. D **40**, 54 (1989); W. Beenakker, W. L. van Neerven, R. Meng, G. A. Schuler, and J. Smith, Nucl. Phys. **B351**, 507 (1991); M. L. Mangano, P. Nason, and G. Ridolfi, Nucl. Phys. **B373**, 295 (1992).
[40] W. Bernreuther, A. Brandenburg, Z. G. Si, and P. Uwer, Nucl. Phys. **B690**, 81 (2004).
[41] G. Corcella *et al.*, arXiv:hep-ph/0210213.
[42] S. Frixione, P. Nason, and B. R. Webber, J. High Energy Phys. 08 (2003) 007.
[43] S. Frixione, E. Laenen, P. Motylinski, and B. R. Webber, J. High Energy Phys. 04 (2007) 081.
[44] U. Baur, Phys. Rev. D **75**, 013005 (2007).
[45] F. Hubaut, E. Monnier, P. Pralavorio, K. Smolek, and V. Simak, Eur. Phys. J. C **44S2**, 13 (2005).
[46] R. K. Ellis and S. Veseli, Phys. Rev. D **60**, 011501 (1999); F. Febres Cordero, L. Reina, and D. Wackeroth, Phys. Rev. D **74**, 034007 (2006).
[47] J. Campbell and R. K. Ellis, Phys. Rev. D **65**, 113007 (2002); J. Campbell, R. K. Ellis, and D. L. Rainwater, Phys. Rev. D **68**, 094021 (2003).
[48] T. Stelzer, Z. Sullivan, and S. Willenbrock, Phys. Rev. D **56**, 5919 (1997); B. W. Harris, E. Laenen, L. Phaf, Z. Sullivan, and S. Weinzierl, Phys. Rev. D **66**, 054024 (2002); G. Bordes and B. van Eijk, Nucl. Phys. **B435**, 23 (1995); Q. H. Cao, R. Schwienhorst, J. A. Benitez, R. Brock, and C. P. Yuan, Phys. Rev. D **72**, 094027 (2005).
[49] M. C. Smith and S. Willenbrock, Phys. Rev. D **54**, 6696 (1996); Q. H. Cao and C. P. Yuan, Phys. Rev. D **71**, 054022 (2005); Q. H. Cao, R. Schwienhorst, and C. P. Yuan, Phys. Rev. D **71**, 054023 (2005).
[50] Z. Sullivan, Phys. Rev. D **70**, 114012 (2004); **72**, 094034 (2005); J. Campbell, R. K. Ellis, and F. Tramontano, Phys. Rev. D **70**, 094012 (2004).
[51] J. Campbell, R. K. Ellis, F. Maltoni, and S. Willenbrock, Phys. Rev. D **75**, 054015 (2007).
[52] J. Campbell and F. Tramontano, Nucl. Phys. **B726**, 109 (2005).
[53] F. Maltoni and T. Stelzer, J. High Energy Phys. 02 (2003) 027; J. Alwall *et al.*, J. High Energy Phys. 09 (2007) 028.
[54] J. Campbell and R. K. Ellis, http://mcfm.fnal.gov.
[55] J. F. Owens, Phys. Rev. D **21**, 742 (1980).
[56] T. Sjostrand, S. Mrenna, and P. Skands, J. High Energy Phys. 05 (2006) 026.
[57] J. Conway, http://www.physics.ucdavis.edu/~conway/research/software/pgs/ pgs4-general.htm.
[58] J. E. Huth *et al.*, in *Proceedings of Research Directions For the Decade: Snowmass 1990*, edited by (World Scientific, Singapore, 1992), p. 134.
[59] S. Catani, Y. L. Dokshitzer, and B. R. Webber, Phys. Lett. B **285**, 291 (1992); S. D. Ellis and D. E. Soper, Phys. Rev. D **48**, 3160 (1993); S. Catani, Y. L. Dokshitzer, M. H. Seymour, and B. R. Webber, Nucl. Phys. **B406**, 187 (1993).
[60] G. C. Blazey *et al.*, arXiv:hep-ex/0005012; M. Albrow *et al.*, arXiv:hep-ph/0610012.
[61] M. Strassler, PHENO07, Madison, WI, 2007.